bioRxiv preprint doi: https://doi.org/10.1101/2019.12.21.885863; this version posted December 23, 2019. The copyright holder for this preprint (which was not certified by peer review) is the author/funder, who has granted bioRxiv a license to display the preprint in perpetuity. It is made available under aCC-BY-NC 4.0 International license.

OBERON3 and SUPPRESSOR OF MAX2 1-LIKE proteins form a regulatory module specifying phloem identity

Eva-Sophie Wallner[1,3], Nina Tonn[1], Friederike Wanke[2], Vadir Lopéz-Salmerón[1,4], Michael Gebert[1], Christian Wenzl[1], Jan U. Lohmann[1], Klaus Harter[2], Thomas Greb[1]*

[1]Centre for Organismal Studies (COS), Heidelberg University, 69120 Heidelberg, Germany

[2]Center for Plant Molecular Biology (ZMBP), University of Tübingen, 72076 Tübingen, Germany

[3]Current address: Gilbert Biological Sciences, Stanford University, Stanford, CA 94305-5020, USA

[4]Current address: BD Bioscience, 69126 Heidelberg, Germany

*Corresponding author. Tel.: +49 6221 54 5524; Fax: +49 6221 54 6424; Email: thomas.greb@cos.uni-heidelberg.de

bioRxiv preprint doi: https://doi.org/10.1101/2019.12.21.885863; this version posted December 23, 2019. The copyright holder for this preprint (which was not certified by peer review) is the author/funder, who has granted bioRxiv a license to display the preprint in perpetuity. It is made available under aCC-BY-NC 4.0 International license.

Abstract

The phloem tissue mediates long-distance transport of energy metabolites along plant bodies and, therefore, is central for plant performance. However, mechanisms initiating the transition of undifferentiated stem cells to cells specialized in metabolite transport are unknown. Here we identify the ubiquitously expressed PHD-finger protein OBERON3 (OBE3) to be essential for phloem formation. We show that OBE3 directly interacts with the SUPPRESSOR OF MAX2 1-LIKE 5 (SMXL5) protein specifically expressed during early phloem development. Both proteins co-localize in nuclei of phloem stem cells and, together with the *SMXL5* homologs *SMXL3* and *SMXL4*, promote the establishment of phloem-specific cellular signatures in a cell-autonomous manner. These signatures include expression of *OCTOPUS* (*OPS*), *BREVIS RADIX* (*BRX*), *BARELY ANY MERISTEM3* (*BAM3*), and *COTYLEDON VASCULAR PATTERN2* (*CVP2*) genes acting as mediators of phloem differentiation. Consistently, genetic analyses show that *SMXL5* acts upstream and independently of *OPS* and *BRX* functions. Based on our findings, we conclude that the formation of an OBE3/SMXL5 protein complex specifically in nuclei of early phloem cells is essential for establishing a phloem-specific developmental program.

Keywords: sieve element, Arabidopsis thaliana, root, stem cell

bioRxiv preprint doi: https://doi.org/10.1101/2019.12.21.885863; this version posted December 23, 2019. The copyright holder for this preprint (which was not certified by peer review) is the author/funder, who has granted bioRxiv a license to display the preprint in perpetuity. It is made available under aCC-BY-NC 4.0 International license.

INTRODUCTION

Growth and body shape of multicellular organisms largely depend on a functional long-distance transport of energy metabolites to fuel stem cell activity. In plants, sugars are photosynthetically produced in source organs, such as leaves, and delivered via the phloem to sink organs where they are allocated to storage tissues or stem cell niches, such as the root apical meristem (RAM) (Oparka and Turgeon 1999; De Schepper et al. 2013). The dividing stem cells of the RAM are located next to a mostly dormant organizer, known as quiescent center (QC) (van den Berg et al. 1997). These stem cells divide and differentiate in a strictly controlled manner to give rise to two phloem poles which ensure a steady energy supply to the RAM during root growth (Rodriguez-Villalon et al. 2014; Wallner et al. 2017). One phloem pole comprises a protophloem and a metaphloem strand, each forming a sieve element (SE) and a companion cell (CC) lineage (Lucas et al. 2013). During differentiation, SEs degrade most of their organelles to build connected sieve tubes for intracellular allocation of sugars, hormones, proteins and RNAs (Furuta et al. 2014). This is why functional SEs are metabolically sustained by CCs via intercellular channels named plasmodesmata (Ross-Elliott et al. 2017). Underlining the importance of the phloem, defects in protophloem development cause root growth defects, possibly, as a consequence of RAM starvation (Depuydt et al. 2013; Rodriguez-Villalon et al. 2014).

Due to the remarkable transition of phloem stem cells to cells holding an extreme degree of specialization, gaining insights into phloem formation and identifying its molecular regulators is highly instructive for our general understanding of cell fate regulation and differentiation. Moreover, due to the extreme importance of the phloem for plant growth and physiology, revealing mechanisms of phloem formation holds great promises for crop production and may increase our understanding of plant evolution and of the adaptation to environmental conditions. Importantly, although several genes, including *OCTOPUS (OPS), BREVIS RADIX (BRX), BARELY ANY MERISTEM3 (BAM3), and COTYLEDON VASCULAR*

bioRxiv preprint doi: https://doi.org/10.1101/2019.12.21.885863; this version posted December 23, 2019. The copyright holder for this preprint (which was not certified by peer review) is the author/funder, who has granted bioRxiv a license to display the preprint in perpetuity. It is made available under aCC-BY-NC 4.0 International license.

PATTERN2 (CVP2), regulating different aspects of phloem formation have been characterized (Bonke et al. 2003; Depuydt et al. 2013; Rodriguez-Villalon et al. 2014; Anne et al. 2015; Rodriguez-Villalon et al. 2015; Hazak et al. 2017; Marhava et al. 2018), those genes seem to act downstream of phloem specification leaving the question open of how a phloem-specific developmental program is initiated.

Recently, a central role of the SUPPRESSOR OF MAX2 1-LIKE (SMXL) protein family members SMXL3, SMXL4 and SMXL5 in phloem formation was revealed (Wallner et al. 2017; Wu et al. 2017; Cho et al. 2018; Wallner et al. 2020). SMXL proteins are well-conserved nuclear localized developmental regulators and, in *Arabidopsis thaliana* (Arabidopsis), form a protein family of eight members sub-divided into different sub-clades based on phylogeny and function (Zhou et al. 2013; Soundappan et al. 2015; Liang et al. 2016; Wallner et al. 2016; Walker and Bennett 2017). While SMAX1 and SMXL2 are targeted for degradation by the karrikin signaling pathway to regulate germination and hypocotyl growth (Stanga et al. 2013; Stanga et al. 2016), SMXL6, SMXL7, and SMXL8 are proteolytic targets of strigolactone signaling, which is a hormonal pathway regulating shoot and root branching (Soundappan et al. 2015; Wang et al. 2015; Liang et al. 2016). In comparison, SMXL3/4/5 proteins act independently from both strigolactone and karrikin signaling as central regulators of phloem formation (Wallner et al. 2017). Their redundant and dose-dependent functions become obvious in double and triple mutants which are completely deprived of protophloem formation within the RAM resulting in root growth termination a few days after germination (Wallner et al. 2017). Despite their fundamental role in (proto)phloem formation the molecular mechanism of SMXL3/4/5 proteins remained obscure.

In contrast to SMXL proteins whose activity is spatially highly restricted, OBERONs (OBEs) are a family of four ubiquitously expressed, nuclear-localized proteins essential for tissue specification and meristem maintenance starting from the earliest stages of embryo

bioRxiv preprint doi: https://doi.org/10.1101/2019.12.21.885863; this version posted December 23, 2019. The copyright holder for this preprint (which was not certified by peer review) is the author/funder, who has granted bioRxiv a license to display the preprint in perpetuity. It is made available under aCC-BY-NC 4.0 International license.

development (Saiga et al. 2008; Thomas et al. 2009; Saiga et al. 2012; Lin et al. 2016). This role is reflected by mutants deficient for either of the two *OBE* sub-families which are embryo lethal (Saiga et al. 2008; Thomas et al. 2009; Saiga et al. 2012). In the shoot apical meristem (SAM), *OBE3* (also known as *TITANIA1* (*TTA1*)), interacts genetically with the homeobox transcription factor gene *WUSCHEL* (*WUS*) in stem cell regulation (Lin et al. 2016). Additionally, *OBE1* and *OBE2* are associated with vascular patterning in the embryo (Thomas et al. 2009). Interestingly, OBEs carry a highly conserved plant homeodomain (PHD)-finger domain known to bind di- and trimethylated histone H3 allowing recruitment of chromatin remodeling complexes and transcription factors (Sanchez and Zhou 2011). Indeed, OBE proteins show chromatin binding and remodeling activities important for root initiation during embryogenesis (Saiga et al. 2008; Saiga et al. 2012). Taken together, OBEs have versatile roles associated with cell fate regulation in plants (Saiga et al. 2008; Thomas et al. 2009; Saiga et al. 2012; Lin et al. 2016) but, as for SMXL proteins, their specific roles in distinct tissues and their mode of action is unknown.

Here, we report that OBE3 and SMXL5 proteins physically interact with each other forming a functional unit during protophloem formation in the RAM. Identified in a yeast two-hybrid screen using SMXL5 as a bait, we provide evidence that SMXL5 and OBE3 proteins interact in yeast and *in planta*. We also elucidate a functional interaction between *OBE3* and *SMXL3/4/5* genes during protophloem development in the root. Just like *SMXL3/4/5, OBE3* is an essential component during protophloem initiation and differentiation. By characterizing the *SMXL3/4/5-OBE3* interaction we provide insights into the molecular network of (proto)phloem formation in plants and propose that the *SMXL3/4/5-OBE3*-dependent establishment of a distinct chromatin profile is an essential step during phloem specification.

bioRxiv preprint doi: https://doi.org/10.1101/2019.12.21.885863; this version posted December 23, 2019. The copyright holder for this preprint (which was not certified by peer review) is the author/funder, who has granted bioRxiv a license to display the preprint in perpetuity. It is made available under aCC-BY-NC 4.0 International license.

RESULTS

Early phloem markers are less active in *smxl4;smxl5* mutants

To position the function of the *SMXL4* and *SMXL5* genes within the process of phloem formation, we introgressed a series of developmental markers visualizing early steps of phloem formation (Rodriguez-Villalon 2016) into the *smxl4;smxl5* double mutant background. Although showing severe defects in protophloem formation, *smxl4;smxl5* is viable and can be propagated in contrast to the *smxl3;smxl4;smxl5* triple mutant, which is devoid of phloem tissues and seedling lethal (Wallner et al. 2017). Comparison of wild type and *smxl4;smxl5* root tips two days after germination when the overall anatomy of the *smxl4;smxl5* RAM is not yet affected by phloem defects (Wallner et al. 2017), showed that *OPS:OPS-GFP, BRX:BRX-CITRINE*, *BAM3:BAM3-CITRINE*, or *CVP2:NLS-VENUS* marker activities (Rodriguez-Villalon et al. 2014) were reduced or not detectable in *smxl4;smxl5* plants (Figure 1, A-H). This reduction was found along the entire strand of the developing protophloem and included SE-procambium stem cells located immediately proximal to the quiescent center (QC). In these founder cells of the phloem tissuefounder cells, we observed accumulation of OPS-GFP and BRX-CITRINE fusion proteins in wild type which was hardly detectable in *smxl4;smxl5* double mutants (Figure 1, I-P). In contrast to markers associated with early stages of phloem development, activity of the *ALTERED PHLOEM DEVELOPMENT* (*APL*) promoter marking differentiating SEs and CCs in wild type (Bonke et al. 2003) was not detectable in root tips of *smxl4;smxl5* mutants (Supplementary Figure 1) similar to *CALS7:H2B-YFP*, a phloem differentiation marker tested previously (Wallner et al. 2017). These observations argued for an early role of *SMXL4* and *SMXL5* in establishing a general phloem-specific developmental program including *OPS*, *BRX*, *BAM3*, and *CVP2* gene activities.

bioRxiv preprint doi: https://doi.org/10.1101/2019.12.21.885863; this version posted December 23, 2019. The copyright holder for this preprint (which was not certified by peer review) is the author/funder, who has granted bioRxiv a license to display the preprint in perpetuity. It is made available under aCC-BY-NC 4.0 International license.

Early activity of *SMXL* genes upstream of *OPS* and *BRX* is required for phloem formation

To challenge this conclusion, we tested the capacity of *SMXL5* to restore protophloem formation when expressed under the control of promoters active during different phases of protophloem development (Rodriguez-Villalon 2016) by using root length as a fast and efficient read-out for phloem defects (Depuydt et al. 2013; Wallner et al. 2017). Supporting the need of *SMXL5* activity during early phases of phloem development, reduced root length usually found in *smxl4;smxl5* mutants was not observed when they expressed *SMXL5* under the control of the early *OPS*, *BAM3*, or *CVP2* promoters (Figure 2A, Supplementary Figure 1). Moreover, SE formation was restored in these backgrounds (Supplementary Figure 1). In contrast, driving *SMXL5* expression by the *APL* promoter did not lead to restoration of root length or SE formation (Figure 2A, Supplementary Figure 1). These results showed that the *SMXL5* function mediated by residual activity of early phloem-related promoters in *smxl4;smxl5* mutants is sufficient to stabilize phloem development.

To see whether the reduced activity of regulators like *BRX* is causative for reduced root length of *smxl4;smxl5* double mutants, we expressed *BRX-VENUS* in *smxl4;smxl5* mutant backgrounds under the control of the early protophloem-specific *SMXL4* promoter (Supplementary Figure 1F) (Wallner et al. 2017). Indeed, root length of *SMXL4:BRX-VENUS/smxl4;smxl5* lines was comparable to the length of wild type roots (Figure 2A) indicating that *BRX* acts downstream of *SMXL4* and that reduced *BRX* activity is one reason for disturbed phloem development in *smxl4;smxl5* mutants. Further supporting a role of the *SMXL4* and *SMXL5* genes upstream of *OPS*, visualization of SMXL4 and SMXL5 proteins in *OPS*-deficient backgrounds by respective reporters (Wallner et al. 2017) did neither reveal a reduced level nor altered localization of SMXL4 or SMXL5 proteins in early protophloem cells (Figure 2, B-E). This suggested that in contrast to a positive effect of *SMXL4* and *SMXL5* on the activity of *OPS* and *BRX* genes (Figure 1), *OPS* was not important for stimulating *SMXL4* or *SMXL5* activity during early steps of phloem formation.

bioRxiv preprint doi: https://doi.org/10.1101/2019.12.21.885863; this version posted December 23, 2019. The copyright holder for this preprint (which was not certified by peer review) is the author/funder, who has granted bioRxiv a license to display the preprint in perpetuity. It is made available under aCC-BY-NC 4.0 International license.

SMXL* genes act on different steps of phloem formation than *OPS* and *BRX

To further test our interpretation that *SMXL* genes on the one side and *OPS* and *BRX* on the other side act on different steps of phloem development, we investigated their genetic interaction. The OPS protein is required for SE formation in the protophloem by counteracting the BAM3/CLAVATA3/ESR-related 45 (CLE45) pathway (Breda et al. 2019). Due to enhanced activity of the BAM3/CLE45 pathway, *ops* mutants develop 'gap cells' within protophloem strands in which SE establishment fails (Truernit et al. 2012; Rodriguez-Villalon et al. 2014). Interestingly, root length of *ops;smxl5* double mutants was similarly reduced as in *smxl4;smxl5* double mutants although *smxl5* single mutants were not affected and *ops* single mutants were very variable in this regard (Figure 3A). This finding suggested an additive effect of the *SMXL* and the *OPS*-dependent pathways on phloem formation. Indeed, when phloem development was carefully analyzed in the respective mutant backgrounds, we observed a variation of phloem defects in *ops* single mutants ranging from the appearance of gap cells to the complete absence of SEs in a small fraction of plants (Figure 3B, Supplementary Figure 2). In comparison, 60 % of the *ops;smxl5* mutants displayed complete SE deficiency demonstrating that both genes contribute to a robust phloem development. A similar trend was observed for *brx;smxl5* double mutants. Like *OPS*, the *BRX* gene ensures continues SE formation in this case, however, by downregulation of *BAM3* transcription and steepening the auxin gradient in developing phloem cells (Scacchi et al. 2010; Depuydt et al. 2013; Marhava et al. 2018; Marhava et al. 2019). Similar to *ops;smxl5* double mutants, *brx;smxl5* double mutants developed shorter roots than *brx* and *smxl5* single mutants and largely failed to differentiate SE (Figure 3A, Supplementary Figure 3). Importantly, in *ops;smxl5* plants which developed SEs, gap cell formation was comparable to *ops* and *brx* single mutants (Figure 3B, Supplementary Figures 1). Together, these observations suggested that although all genes are important for a stable phloem formation, *SMXL* genes and *OPS* and *BRX* genes regulate different steps during phloem formation.

bioRxiv preprint doi: https://doi.org/10.1101/2019.12.21.885863; this version posted December 23, 2019. The copyright holder for this preprint (which was not certified by peer review) is the author/funder, who has granted bioRxiv a license to display the preprint in perpetuity. It is made available under aCC-BY-NC 4.0 International license.

SMXL5 proteins interact with OBE3 proteins in nuclei of plant cells

To find indications for how SMXL proteins fulfil their role, we isolated interacting proteins by a Yeast-Two-Hybrid-based screen of a cDNA expression library generated from *Arabidopsis* seedlings. As a bait, we used the full length SMXL5 protein (Legrain et al. 2001; Cifuentes-Esquivel et al. 2013) and tested 84 million individual protein-protein interactions. As a result, we isolated 24 independent cDNA clones of the *OBE3* gene. Interaction between SMXL5 and OBE3 proteins in yeast was confirmed when testing the interaction directly. Yeast colonies co-expressing BD-SMXL5 and AD-OBE3 protein fusions grew on high-stringency medium selecting for protein-protein interaction, while transformants expressing BD-SMXL5 or AD-OBE3 alone did not grow (Figure 4A) indicating that BD-SMXL5 and AD-OBE3 proteins interacted in yeast.

To confirm protein-protein interaction, we transiently expressed SMXL5 fused to a triple human influence hemagglutinin (HA) affinity tag and OBE3 fused to a six fold c-Myc epitope tag in *Nicotiana benthamiana* (*N. benthamiana*) leaves under the control of the Cauliflower Mosaic Virus (CaMV) *35S* promoter (Benfey and Chua 1990). In raw protein extracts before ('input') and after ('unbound') immunoprecipitation (IP) using HA-affinity beads and in the precipitate itself ('IP: α HA'), the SMXL5-3xHA protein was detected with the expected size of approximately 120 kDa in Western analyses (Figure 4B). Importantly, the 6xMyc-OBE3 fusion protein co-immunoprecipitated with the SMXL5-3xHA protein and did not show unspecific binding to the HA-affinity beads, indicating that SMXL5-3xHA and 6xMyc-OBE3 proteins interacted in plant cells. Of note, the calculated size of 100 kDa for the 6xMyc-OBE3 protein exceeded the expected size of approximately 92 kDa suggesting that the 6xMyc-OBE3 protein is posttranslationally modified.

bioRxiv preprint doi: https://doi.org/10.1101/2019.12.21.885863; this version posted December 23, 2019. The copyright holder for this preprint (which was not certified by peer review) is the author/funder, who has granted bioRxiv a license to display the preprint in perpetuity. It is made available under aCC-BY-NC 4.0 International license.

To compare the sub-cellular localizations of SMXL5 and OBE3 proteins, we transiently expressed the SMXL5 protein fused to monomeric Cherry (SMXL5-mCherry) together with the OBE3 protein fused to monomeric GFP (OBE3-GFP) likewise in *N. benthamiana* leaves. Initially, nuclear localization of the OBE3 protein was confirmed by co-expressing OBE3-GFP with mCherry fused to a nuclear localization signal (mCherry-NLS). Interestingly, while the mCherry-NLS signal was homogenously distributed within the nucleus, the OBE3-GFP protein appeared in nuclear speckles (Figure 4, C-E). Co-expression of SMXL5-mCherry and OBE3-GFP revealed a co-localization of both proteins within a sub-domain of the nucleus (Figure 4, F-H). This structure was clearly distinct from the whole nucleus highlighted by *mGFP-mCherry-NLS* fusion protein expressed under the control of the *ubiquitin 10* (*UBI10*) promoter (Figure 4, I-K).

We next evaluated our yeast two-hybrid and co-immunoprecipitation data by performing Förster resonance energy transfer (FRET)-fluorescence lifetime imaging microscopy (FLIM) analysis as a cell biological assay for protein-protein association in transiently transformed *N. benthamiana* epidermal leaf cells. The FRET-FLIM analysis detected a significant change in the lifetime of the donor OBE3-mGFP fusions in the nucleus when co-expressed with SMXL5-mCherry (Figure 4L, M). In contrast, we did not observe significant mGFP lifetime changes when OBE-mGFP was expressed with NLS-mCherry (Figure 4L, M). Taken these observations together, we thus concluded that OBE3 interacts with SMXL5 in nuclei of living plant cells.

The *OBE3* gene acts together with *SMXL3*, *SMXL4* and *SMXL5*

Since physical interaction and subcellular co-localization suggested a common action of SMXL5 and OBE3 proteins in plants, we investigated whether the corresponding genes are functionally connected by using again root length as a first read-out for potential phloem defects. As before, *smxl4;smxl5* double mutants were short rooted, while root lengths of *smxl4*

bioRxiv preprint doi: https://doi.org/10.1101/2019.12.21.885863; this version posted December 23, 2019. The copyright holder for this preprint (which was not certified by peer review) is the author/funder, who has granted bioRxiv a license to display the preprint in perpetuity. It is made available under aCC-BY-NC 4.0 International license.

and *smxl5* single mutants were similar to wild type (Wallner et al. 2017) (Figure 5, A and B). Similarly, roots from *obe1, obe2*, *obe3* and *obe4* single mutants resembled wild type roots, while *smxl4;obe3, smxl5;obe3* and *smxl3;obe3* double mutants had short roots just as *smxl4;smxl5* (Figure 5, A-D) suggesting a concerted action of *OBE3* and *SMXL3*, *SMXL4* or *SMXL5* genes during primary root growth. Interestingly, we only detected a genetic interaction between *SMXL3/4/5* and *OBE3* and not between *SMXL4/5* and the other *OBE* family members (Supplementary Figure 4).

OBE3 **locally promotes early stages of phloem development**

Because reduced root length of *obe3;smxl* double mutants suggested a role of *OBE* genes in phloem development, we next tested whether *OBE* genes are expressed in developing phloem cells by comparing the activity pattern of a translational *SMXL4:SMXL4-YFP* reporter (Wallner et al. 2017) with patterns of translational *OBE3:OBE3-GFP* and *OBE4:OBE4-GFP* reporters (Saiga et al. 2012) (Figure 6, A-D). As a marker to identify protophloem cell lineages, we again used increased cell wall staining by Direct Red 23 based on the prominent cell walls of SE cells (Figure 6, A-C). As reported previously (Wallner et al. 2017), analysis of *SMXL4:SMXL4-YFP* reporter lines revealed SMXL4-YFP protein accumulation specifically in nuclei of developing protophloem cells (Figure 6A). In comparison, *OBE3:OBE3-GFP* and *OBE4:OBE4-GFP* reporters showed OBE3-GFP and OBE4-GFP protein accumulation in nuclei of all cell types of the root tip including developing protophloem cells (Figure 6, B-C). Considering that SMXL3 and SMXL5 proteins are also present in those cells (Wallner et al. 2017), we thus concluded that SMXL3/4/5 and OBE proteins had the potential to interact during early phloem formation. Of note, we could not detect differences in activity patterns between *OBE3:OBE3-GFP* and *OBE4:OBE4-GFP* reporters which argues against the fact that differences in expression are the reason why *OBE3*, but not *OBE4*, genetically interacted with *SMXL3/4/5* genes during root growth.

bioRxiv preprint doi: https://doi.org/10.1101/2019.12.21.885863; this version posted December 23, 2019. The copyright holder for this preprint (which was not certified by peer review) is the author/funder, who has granted bioRxiv a license to display the preprint in perpetuity. It is made available under aCC-BY-NC 4.0 International license.

To evaluate whether growth defects observed in *smxl;obe3* roots are correlated with the same type of protophloem defects observed in *smxl4;smxl5* mutants, we analyzed phloem development in the respective genetic backgrounds. During protophloem development, SE procambium-precursors divide tangentially to give rise to procambium and SE precursor cells. After 2-3 anticlinal divisions, SE precursor cells divide again tangentially to initiate meta- and protophloem cell files that subsequently undergo gradual differentiation (Figure 6D) (Wallner et al. 2017). Our analysis revealed that in *obe3* mutant both the tangential cell divisions and the onset of SE differentiation appeared as in wild type roots (Figure 6, E, F, K). In contrast, in *smxl4;obe3* and *smxl5;obe3* mutants, the onset of the second tangential division initiating meta- and protophloem cell lineages was similarly delayed as in *smxl4;smxl5* mutants and the enhanced mPS-PI staining visualizing differentiated SEs was likewise absent (Figure 6 G-I, K and Supplementary Figure 5). This observation demonstrated that, like the more locally expressed *SMXL3/4/5* genes, *OBE3* substantially contributes to phloem formation. Moreover, because respective single mutants did not show these defects (Figure 6 and Supplementary Figure 5), we concluded that *OBE3* or *SMXL5*-deficient plants represent sensitized backgrounds for the functional loss of the other regulator. Of note, protophloem formation in *smxl5;obe4* double mutants was indistinguishable from wild type in accordance with the wild type-like root growth of those plants (Figure 6, E and J).

Because *OBE3* is broadly expressed, phloem defects observed in *smxl5;obe3* mutants could arise due to a function of *OBE3* in other tissues than developing phloem cells, which would contradict a direct interaction of SMXL5 and OBE3 proteins. To address this concern and to determine whether *OBE3* acts cell-autonomously on phloem development, we expressed *OBE3* exclusively in developing phloem cells by introducing a transgene driving an OBE3-turquoise fusion protein under the control of the *SMXL5* promoter (*SMXL5:OBE3-turquoise*) into a *smxl5;obe3* double mutant background. Microscopic analysis of root tips from *smxl5;obe3/SMXL5:OBE3-turquoise* lines confirmed the presence of the OBE3-turquoise protein in nuclei of developing protophloem cells (Figure 7, A and B) as described for the

bioRxiv preprint doi: https://doi.org/10.1101/2019.12.21.885863; this version posted December 23, 2019. The copyright holder for this preprint (which was not certified by peer review) is the author/funder, who has granted bioRxiv a license to display the preprint in perpetuity. It is made available under aCC-BY-NC 4.0 International license.

SMXL5 protein expressed under the control of the same promoter (Wallner et al. 2017). When comparing *smxl5;obe3/SMXL5:OBE3-turquoise* lines with *smxl5;obe3* mutants, we observed that expression of *OBE3-turquoise* within the *SMXL5* domain was indeed sufficient to restore root length in *smxl5;obe3* double mutants (Figure 7, C and D). Additionally, enhanced counter staining in mature protophloem, which indicated that SE differentiation, was recovered in *smxl5;obe3* carrying the *SMXL5:OBE3-turquoise* transgene (Figure 7, A and B). To see whether the predominant reduction of *OBE3* activity is sufficient for generating phloem defects, we designed two independent artificial microRNAs targeting the *OBE3* mRNA (*obe3-miRNAs*) (Schwab et al. 2006) which we expressed under the control of the *SMXL5* promoter in *smxl5* mutant plants. As expected, the majority of those plants was short rooted, indicating that *OBE3* knock-down within the *SMXL5* domain was sufficient to evoke a *smxl5;obe3*-like phenotype in *smxl5* mutants (Figure 7, C and D). We thus concluded that *OBE3* fulfils a local and cell autonomous role in protophloem formation.

bioRxiv preprint doi: https://doi.org/10.1101/2019.12.21.885863; this version posted December 23, 2019. The copyright holder for this preprint (which was not certified by peer review) is the author/funder, who has granted bioRxiv a license to display the preprint in perpetuity. It is made available under aCC-BY-NC 4.0 International license.

DISCUSSION

Cell type specification is fundamental for establishing multicellular organisms and, in recent years, the phloem has become an instructive model for studying this aspect in plants (Anne and Hardtke 2017; Blob et al. 2018). With our study we provide new insights into the regulation of (proto)phloem formation by revealing a role of the putative chromatin remodeling protein OBE3 (Saiga et al. 2012) and a direct interaction between the OBE3 protein and the central phloem regulator SMXL5. Based on our findings, we propose that SMXL proteins fulfil their role in phloem formation by establishing a distinct chromatin signature important for establishing phloem identity.

SMXL3/4/5 and OBE3 proteins act together on early stages of phloem development

SMXL3/4/5 and OBE3 proteins are already expressed in phloem stem cells (Wallner et al. 2017), which was so far not described for other phloem regulators (Blob et al. 2018). Unexpectedly, we detected OPS and BRX protein accumulation already in those stem cells raising the question of functional interdependance. The positive effect of *SMXL4* and *SMXL5* gene functions on OPS and BRX protein accumulation in those and more mature phloem cells suggests, however, that *SMXL* genes are required for the establishment of a phloem-specific developmental program including *OPS* and *BRX* gene activities. The different subcellular localization of OPS, BRX and BAM3 proteins on the one side and SMXL proteins on the other side argues against a more interconnected function of both groups of regulators. The conclusion that both groups act on different aspects of phloem formation is furthermore supported by our genetic analyses which revealed a combination of distinct phloem defects in respective double mutants. Here, we propose that SMXL proteins fulfil their role in the nucleus of phloem stem cells and beyond by direct interaction with OBE3. In fact, the *SMXL3/4/5-OBE3* interaction seems to be a prerequisite for both the initiation of phloem cell fate and a timely onset of differentiation. On the genetic level, *smxl4;obe3*, *smxl5;obe3* and the *smxl4;smxl5* double mutants share the same phloem defects meaning that they are deprived of protophloem

bioRxiv preprint doi: https://doi.org/10.1101/2019.12.21.885863; this version posted December 23, 2019. The copyright holder for this preprint (which was not certified by peer review) is the author/funder, who has granted bioRxiv a license to display the preprint in perpetuity. It is made available under aCC-BY-NC 4.0 International license.

formation within the RAM. Other reported phloem mutants have either problems with completing phloem differentiation in general, which is the case in mutants of the *ALTERED PHLOEM DEVELOPMENT* (*APL*) gene (Bonke et al. 2003; Truernit et al. 2008; Kondo et al. 2016), or they develop 'gap cells' in which SE-differentiation is disturbed as in *ops* or *brx* single or in *cvp2;cvp2-like1* (*cvl1*) double mutants (Depuydt et al. 2013; Anne et al. 2015; Rodriguez-Villalon et al. 2015; Marhava et al. 2018; Breda et al. 2019). In contrast, *smxl5;obe3*, *smxl4;obe3* and multiple mutants of the *SMXL3/4/5* genes show absence of all morphological hallmarks of phloem formation within the RAM. This suggests that *SMXL3/4/5* and *OBE3* act together on the establishment of a phloem-specific developmental program. Interestingly, complete suppression of protophloem formation was so far only reported for roots treated with certain CLAVATA3/ESP-RELATED (CLE) peptides, such as CLE45, which signal through the leucine-rich repeat receptor like kinase BAM3 and the pseudokinase CORYNE (CRN) (Depuydt et al. 2013; Hazak et al. 2017). Of note, the formation of 'gap cells' in *ops* or *brx* mutants is suppressed in *BAM3*-deficient backgrounds (Rodriguez-Villalon et al. 2014). This, on the one hand, indicates a molecular interplay between OPS/BRX and BAM3-CLE45, and, on the other hand, shows that none of those factors is required to obtain protophloem cell identity and proper differentiation in the first place (Depuydt et al. 2013; Rodriguez-Villalon et al. 2014). Future work will show how the SMXL3/4/5/OBE3 module interacts with these signaling components.

A putative role of a SMXL3/4/5/OBE3 protein complex in chromatin remodeling

PHD-finger motifs as carried by the OBE3 protein are known to be epigenetic readers binding to histone H3 tails carrying distinct post-translational modifications such as trimethylation of lysine 4 (H3K4me3) or lysine 9 (H3K9me) marking actively transcribed or silent chromatin regions, respectively (Sanchez and Zhou 2011). Although PHD finger proteins themselves are not necessarily activating or repressing, they can indirectly modify transcription by recruiting chromatin modifying complexes (De Lucia et al. 2008). Indeed, OBE proteins

bioRxiv preprint doi: https://doi.org/10.1101/2019.12.21.885863; this version posted December 23, 2019. The copyright holder for this preprint (which was not certified by peer review) is the author/funder, who has granted bioRxiv a license to display the preprint in perpetuity. It is made available under aCC-BY-NC 4.0 International license.

have been proposed to remodel chromatin structure during embryogenesis and thereby transcriptionally activate RAM initiation factors (Saiga et al. 2012). SMXL proteins share an ethylene-responsive element binding factor-associated amphiphilic repression (EAR) motif which interacts with transcriptional regulators of the TOPLESS (TPL) family (Pauwels et al. 2010). Indeed, the strigolactone signaling mediators SMXL6, SMXL7, SMXL8 and DWARF53 (D53), an SMXL protein from rice, directly interact with TPL-like proteins (Soundappan et al. 2015; Wang et al. 2015; Ma et al. 2017). TPLs are transcriptional co-repressor that can recruit histone deacetylases (HDAC) and, thereby, induce chromatin condensation and transcriptional suppression (Krogan and Long 2009; Ma et al. 2017). In addition to EAR motifs, SMXLs share a conserved double caseinolytic protease (Clp) domain with ATPase activity that resembles heat shock protein 101 (HSP101) (Jiang et al. 2013; Zhou et al. 2013). As recently proposed, the p-loop ATPase domain of D53 fosters the formation of TPL hexamers and the threading of DNA through a central pore of this hexamer inducing nucleosome repositioning and/or higher-order chromatin reorganization (Ma et al. 2017).

Judging from the protein domains and sub-nuclear localization, we hypothesize that SMXL3/4/5 and OBE3 form a protein complex that is involved in chromatin remodeling and/or transcriptional regulation of downstream targets. Similar to the previous report on the OBE3-WUS interaction in the SAM (Lin et al. 2016), we cannot rule out that other OBE family members apart from OBE3 interact with SMXL3/4/5 in protophloem formation. Although all mutant alleles used in this study were reported to be functional knock-outs because multiple mutants show strong embryonic defects (Saiga et al. 2008; Saiga et al. 2012), residual activity of the *OBE1*, *OBE2* or *OBE4* genes might be sufficient to support *SMXL3/4/5* activity. In summary, our study reveals the functional interaction between *SMXL3/4/5* and *OBE3*, an important step in understanding the role of SMXL proteins in phloem formation.

bioRxiv preprint doi: https://doi.org/10.1101/2019.12.21.885863; this version posted December 23, 2019. The copyright holder for this preprint (which was not certified by peer review) is the author/funder, who has granted bioRxiv a license to display the preprint in perpetuity. It is made available under aCC-BY-NC 4.0 International license.

Material and Methods

Arabidopsis thaliana

Genotypes of plant species *Arabidopsis thaliana* (L.) Heynh. of the ecotype Columbia (Col) used for genetic analysis are listed in the Key Resource Table. Sterile seeds were stratified in microcentrifuge tubes containing dH_2O at 4 °C in the dark for 3 days and then sown in rows on ½ Murashige and Skoog (MS) medium-plates supplemented with 1 % sucrose and grown vertically. Seedlings were grown in long day (LD, 16 h light and 8 h dark) conditions at 21 °C for 2-10 days. Flowering plants were transformed by the floral dip method described earlier (Clough and Bent 1998). Seeds were liquid sterilized by 70 % ethanol supplemented with 0.2 % Tween-20 for 15 min, washed twice with 100 % ethanol and air dried under sterile conditions.

Yeast-Two-Hybrid

The yeast-based screen for proteins interacting with SMXL5 was performed by Hybrigenics (Evry, France) as described before (Legrain et al. 2001). The yeast strain *AH109* was used for the yeast two-hybrid assay according to Matchmaker™ Two-Hybrid System 3 (Clontech, Palo Alto) and grown on YPD (full medium) or SD (selective medium)-agar plates for 3-5 days at 28°C, then stored at 4°C and stroked onto new plates every 10 days. Dilution series (OD600 1-0.001) of transformed yeast strains were grown for 3 days on selective medium (SD) -Leu/-Trp/-His/-Ade selecting for protein interaction or SD -Leu/-Trp selecting for the presence of the plasmids. When grown in liquid YPD medium for transformation, yeast was grown over night at 28 °C with shaking at 250 rpm. For expressing the GAL4BD-SMXL5 fusion protein in yeast the open reading frame of the *SMXL5* gene was cloned into XmaI/BamHI sites of the *pGBKT7* plasmid (Clontech, Palo Alto) resulting in *pEW6*. For expressing the GAL4AD-OBE3 fusion protein, the open reading frame of the *OBE3* gene was cloned into XmaI/BamHI sites of the *pGADT7* plasmid (Clontech, Palo Alto) resulting into *pEW11*.

bioRxiv preprint doi: https://doi.org/10.1101/2019.12.21.885863; this version posted December 23, 2019. The copyright holder for this preprint (which was not certified by peer review) is the author/funder, who has granted bioRxiv a license to display the preprint in perpetuity. It is made available under aCC-BY-NC 4.0 International license.

Agrobacterium tumefaciens

The *Agrobacterium tumefaciens* genotypes C58C1: RifR with pSoup plasmid (TetR) or ASE: KanR, CamR with pSoup+ plasmid (TetR) were used for transformation of *Arabidopsis thaliana* or infiltration of *N. benthamiana* leaves and grown at 28 °C over night in liquid YEB medium on a shaker (180 rpm to an OD_{600} > 1) or plated on YEB-plates and grown in an incubator (Fraley et al. 1983; Ashby et al. 1988; Hellens et al. 2000). Antibiotics were used for plasmid selection.

Root length measurements

For measuring root lengths, seedlings were scanned by a commercial scanner and analyzed using ImageJ 1.49d (Schindelin et al. 2012).

Genotyping

Genotyping was performed by PCR using primers listed in Supplementary Table 1. Further information about standard DNA extraction and genotyping can be found in (Wallner 2018).

Transient protein expression in *N. benthamiana*

N. benthamiana plants were used for transient protein expression and grown in the greenhouse at approximately 25 °C and watered daily. Transformed *Agrobacteria* were stored as glycerol stocks and grown in a 10 ml YEB liquid culture prior to use. The densely grown culture was centrifuged at 4000 rpm for 5 min at RT. The supernatant was removed and the pellet was washed with 5 ml induction buffer and re-suspended in 10 ml induction buffer. Culture densities were adjusted to an OD_{600} of 1. Prior to infiltration, these bacterial solutions

bioRxiv preprint doi: https://doi.org/10.1101/2019.12.21.885863; this version posted December 23, 2019. The copyright holder for this preprint (which was not certified by peer review) is the author/funder, who has granted bioRxiv a license to display the preprint in perpetuity. It is made available under aCC-BY-NC 4.0 International license.

were mixed with *Agrobacteria* expressing *35S:P19* in a ratio 1:2 and incubated in the dark for 2-3 h (Voinnet et al. 2003; Scholthof 2006). *N. benthamiana* leaves were infiltrated with the mixtures using a 1 ml syringe (Becton Dickinson S.A., Heidelberg, Germany). Leaves were harvested three days after infiltration.

Protein extraction, immunoprecipitation and Western blot

Infiltrated *N. benthamiana* leaves were frozen in liquid nitrogen and ground by a mortar. Proteins were extracted by mixing the leaf powder 1:1 with extraction buffer (50 mM Na_3PO_4, 150 mM NaCl, 10% glycerol, 5 mM EDTA, 10 mM β-mercaptoethanol, 0.1% triton X-100, 2 mM $NaVO_4$, 2 mM NaF, 20 µM MG-132, 1 mM PMSF, 1x cOmpleteTM Protease Inhibitor Cocktail (Roche; Basel, Switzerland)). Each sample was vortexed for 10 sec and centrifuged at 13000 rpm for 10 min at 4 °C. The protein extract was retrieved by sieving it through a nylon mesh. Protein quantities were measured by Bradford assays according to the manual provided with the Bio-Rad Protein Assay Dye Reagent Concentrate (Bio-Rad Laboratories; Hercules, USA). Proteins were immunoprecipitated by 50 µl Anti-HA MicroBeads (Miltenyi Biotec, Bergisch Gladbach, Germany) after incubation for 2.5 h at 4 °C while slowly rotating. Beads were captured by µ Columns (Miltenyi Biotec, Bergisch Gladbach, Germany) on magnetic stands by following the user manual and washed three times by 200 µl Wash buffer I (extraction buffer without β-mercaptoethanol) and two times by 200 µl Wash buffer II (50 mM Na_3PO_4, 150 mM NaCl, 10% glycerol, 5 mM EDTA). Proteins were eluted by 2x Laemmli buffer (95 °C) and separated by size on a SDS-PAGE with subsequent western blotting. Detailed procedures can be found in (Wallner 2018). SMXL5-3xHA and 6xMyc-OBE3 bands were detected by antibodies Anti-HA-Peroxidase High Affinity (3F10) (Roche; Basel, Switzerland) or c-Myc Antibody (9E10) sc-40 HRP (Santa Cruz Biotechnology, Santa Cruz, USA), respectively and visualized by chemiluminescence agents SuperSignal™ West Femto Maximum Sensitivity Substrate (Thermo-Scientific; Waltham, USA) by an Advanced Fluorescence and ECL Imager (Intas Science Imaging Instruments, Göttingen, Germany).

bioRxiv preprint doi: https://doi.org/10.1101/2019.12.21.885863; this version posted December 23, 2019. The copyright holder for this preprint (which was not certified by peer review) is the author/funder, who has granted bioRxiv a license to display the preprint in perpetuity. It is made available under aCC-BY-NC 4.0 International license.

FRET-FLIM analyses

FRET-FLIM analyses were performed principally as described previously (Ladwig et al. 2015; Arongaus et al. 2018). Briefly, measurements were performed using a Leica TCS SP8 microscope (Leica Microsystems, Germany) equipped with a rapidFLIM unit (PicoQuant). Images were acquired using a 63x/1.20 water immersion objective. For the excitation and emission of fluorescent proteins, the following settings were used: mGFP at excitation 488 nm and emission 500-550 nm; and mCherry at excitation 561 nm and emission 600-650 nm. The lifetime τ [ns] of either the donor only expressing cells or the cells expressing the indicated combinations was measured with a pulsed laser at an excitation light source of 470 nm and a repetition rate of 40 MHz (PicoQuant Sepia Multichannel Picosecond Diode Laser, PicoQuant Timeharp 260 TCSPC Module and Picosecond Event Timer). The acquisition was performed until 500 photons in the brightest pixel were reached. To obtain the GFP fluorescence lifetime, data processing was performed with SymPhoTime software and bi-exponential curve fitting and a correction for the instrument response function. Statistical analysis was carried out using the JMP 14 sofware (JMP, USA).

Direct Red 23 staining

To preserve fluorescent signals in roots, seedlings were fixed in a vacuum chamber for 1 h by 4 % (w/v) PFA dissolved in PBS. The tissue was washed twice by PBS and cleared with ClearSee solution for a minimum of two days according to (Kurihara et al. 2015). Cleared seedlings were stained by 0.01 % (w/v) Direct Red 23 in ClearSee solution for 1 h. Excess staining was removed by clearing once again in pure ClearSee solution for 1 h.

mPS-PI staining

The mPS-PI staining of roots was carried out as described before (Truernit et al. 2008).

bioRxiv preprint doi: https://doi.org/10.1101/2019.12.21.885863; this version posted December 23, 2019. The copyright holder for this preprint (which was not certified by peer review) is the author/funder, who has granted bioRxiv a license to display the preprint in perpetuity. It is made available under aCC-BY-NC 4.0 International license.

Confocal microscopy

For confocal microscopy, TCS SP5 or SP8 microscopes (Leica Microsystems; Mannheim, Germany) were used. GFP signals were excited at excited by an argon laser at 488 nm, collecting the emission between 500-575 nm. YFP was excited by an argon laser at 514 nm and the emission detected in a range of 520-540 nm. DirectRed stained tissue was excited at 561 nm (DPSS laser) and emission was detected at wavelengths >660 nm. mPS-PI stained tissue was excited at 561 nm (DPSS laser) and emission was detected at 590-690 nm.

Molecular cloning and miRNA generation

OPS:SMXL5-VENUS (*pNT52*), *OPS:ER-VENUS* (*pNT53*), *BAM3:SMXL5-VENUS* (*pNT49*), *BAM3:ER-VENUS* (*pNT50*), *CVP2:SMXL5-VENUS* (*pNT16*), *CVP2:ER-VENUS* (*pNT69*), *APL:SMXL5-VENUS* (*pNT10), APL:ER-VENUS (pNT68), SMXL4:BRX-VENUS* (*pNT72*), *SMXL5:OBE3-turquoise* (*pEW72*), *35S:5xc-Myc-OBE3* (*pEW78*), *35S:SMXL5-mCherry* (*pVL122*), *35S:OBE3-mGFP* (*pVL127*), *35S:mCherry-NLS* (*pMG103*) and *UBI10:mGFP-mCherry-NLS* (*pCW194*) constructs were generated by using appropriate modules according to the GreenGate manual described in (Lampropoulos et al. 2013). Destination modules, entry modules, and correlating primers for amplifying DNA fragments for generating entry modules are depicted in Supplementary Table 1. In case reporter proteins were targeted to the endoplasmatic reticulum (ER), they were fused to the appropriate motifs (Haseloff et al. 1997). *miRNAs* targeting *OBE3* transcripts were designed and cloned according to the manual provided by the WMD3 - Web MicroRNA Designer Version 3 (Max Planck Institute for Developmental Biology, Tübingen. http://www.weigelworld.org) with primers listed in Supplementary Table 1. To generate *35S:SMXL5-3xHA* (*pEW33*), the *SMXL5* CDS was amplified by primers listed In Supplementary Table 1 and cloned into BamHI/XbaI sites of *pGreen0229:35S* (Hellens et al. 2000) resulting in *pKG33*. Next, ssDNA sequences coding for 3xHA (Supplementary Table 1) were annealed by gradual cool-down from 80 °C to

bioRxiv preprint doi: https://doi.org/10.1101/2019.12.21.885863; this version posted December 23, 2019. The copyright holder for this preprint (which was not certified by peer review) is the author/funder, who has granted bioRxiv a license to display the preprint in perpetuity. It is made available under aCC-BY-NC 4.0 International license.

50 °C and inserted into vector *pKG33* using BamHI/XmaI sites, resulting in plasmid *pEW31*. Further information about detailed cloning procedures can be found in (Wallner 2018).

Quantification and statistical analyses

Statistical analyses were performed using IBM SPSS Statistics for Windows, Version 22.0. Armonk, NY: IBM Corp or using GraphPad Prism version 6.01 (GraphPad Software, La Jolla, USA). Means were calculated from measurements with sample sizes as indicated in the respective figure legends. In general, all displayed data represents at least three independent, technical repetitions, unlike otherwise indicated. Error bars represent ± standard deviation. All analyzed datasets were prior tested for homogeneity of variances by the Levene statistic. One-way ANOVA was performed, using a confidence interval (CI) of 95% and a post-hoc Tukey HSD for comparisons of five or more data sets of homogenous variances or a post-hoc Tamhane-T2 in case variances were not homogenous. Graphs were generated in GraphPad Prism version 6.01 (GraphPad Software, La Jolla, USA) or in Excel (Microsoft, Redmond, USA).

bioRxiv preprint doi: https://doi.org/10.1101/2019.12.21.885863; this version posted December 23, 2019. The copyright holder for this preprint (which was not certified by peer review) is the author/funder, who has granted bioRxiv a license to display the preprint in perpetuity. It is made available under aCC-BY-NC 4.0 International license.

Acknowledgements

This work was supported by the SFB 1101 to K.H., J.U.L, and T.G. and SFB 873 to J.U.L. and T.G. (Deutsche Forschungsgemeinschaft, DFG), a Heisenberg Professorship (DFG, GR 2104/5-2), and an ERC Consolidator grant (PLANTSTEMS, #647148) to T.G. and a PhD student fellowship of the Cusanuswerk to N.T.. We are grateful to Christian Hardtke (University of Lausanne, Switzerland), Dolf Weijers, Shunsuke Saiga (both at Wageningen University, The Netherlands), Andy Maule (John Innes Centre, UK), Sebastain Wolf and Karin Schumacher (both Heidelberg University, Germany) for providing seed material and constructs.

Author Contributions

Conceived and designed the experiments: EW, NT, FW, VL, KH, TG. Performed experiments: EW, NT, FW, VL, MG, CW, JUL. Analysed the data: EW, NT, FW, KH, TG. Wrote the paper: EW, TG.

Conflict of Interest

The authors declare that they have no conflict of interest.

bioRxiv preprint doi: https://doi.org/10.1101/2019.12.21.885863; this version posted December 23, 2019. The copyright holder for this preprint (which was not certified by peer review) is the author/funder, who has granted bioRxiv a license to display the preprint in perpetuity. It is made available under aCC-BY-NC 4.0 International license.

References

Anne P, Azzopardi M, Gissot L, Beaubiat S, Hematy K, Palauqui JC. 2015. OCTOPUS Negatively Regulates BIN2 to Control Phloem Differentiation in Arabidopsis thaliana. *Current Biology* **25**: 2584-2590.

Anne P, Hardtke CS. 2017. Phloem function and development-biophysics meets genetics. *Curr Opin Plant Biol* **43**: 22-28.

Arongaus AB, Chen S, Pireyre M, Glockner N, Galvao VC, Albert A, Winkler JB, Fankhauser C, Harter K, Ulm R. 2018. Arabidopsis RUP2 represses UVR8-mediated flowering in noninductive photoperiods. *Genes Dev* **32**: 1332-1343.

Ashby AM, Watson MD, Loake GJ, Shaw CH. 1988. Ti plasmid-specified chemotaxis of Agrobacterium tumefaciens C58C1 toward vir-inducing phenolic compounds and soluble factors from monocotyledonous and dicotyledonous plants. *Journal of bacteriology* **170**: 4181-4187.

Benfey PN, Chua NH. 1990. The Cauliflower Mosaic Virus 35S Promoter: Combinatorial Regulation of Transcription in Plants. *Science* **250**: 959-966.

Blob B, Heo JO, Helariutta Y. 2018. Phloem differentiation: an integrative model for cell specification. *J Plant Res* **131**: 31-36.

Bonke M, Thitamadee S, Mähönen AP, Hauser MT, Helariutta Y. 2003. APL regulates vascular tissue identity in Arabidopsis. *Nature* **426**: 181-186.

Breda AS, Hazak O, Schultz P, Anne P, Graeff M, Simon R, Hardtke CS. 2019. A Cellular Insulator against CLE45 Peptide Signaling. *Current biology : CB* **29**: 2501-2508.

Cho H, Cho HS, Nam H, Jo H, Yoon J, Park C, Dang TVT, Kim E, Jeong J, Park S et al. 2018. Translational control of phloem development by RNA G-quadruplex-JULGI determines plant sink strength. *Nature plants* **4**: 376-390.

Cifuentes-Esquivel N, Bou-Torrent J, Galstyan A, Gallemi M, Sessa G, Salla Martret M, Roig-Villanova I, Ruberti I, Martinez-Garcia JF. 2013. The bHLH proteins BEE and BIM positively modulate the shade avoidance syndrome in Arabidopsis seedlings. *The Plant journal : for cell and molecular biology* **75**: 989-1002.

Clough SJ, Bent AF. 1998. Floral dip: a simplified method for Agrobacterium-mediated transformation of Arabidopsis thaliana. *The Plant journal : for cell and molecular biology* **16**: 735-743.

De Lucia F, Crevillen P, Jones AM, Greb T, Dean C. 2008. A PHD-polycomb repressive complex 2 triggers the epigenetic silencing of FLC during vernalization. *Proceedings of the National Academy of Sciences of the United States of America* **105**: 16831-16836.

De Schepper V, De Swaef T, Bauweraerts I, Steppe K. 2013. Phloem transport: a review of mechanisms and controls. *Journal of experimental botany* **64**: 4839-4850.

Depuydt S, Rodriguez-Villalon A, Santuari L, Wyser-Rmili C, Ragni L, Hardtke CS. 2013. Suppression of Arabidopsis protophloem differentiation and root meristem growth by CLE45 requires the receptor-like kinase BAM3. *Proceedings of the National Academy of Sciences of the United States of America* **110**: 7074-7079.

Fraley RT, Rogers SG, Horsch RB, Sanders PR, Flick JS, Adams SP, Bittner ML, Brand LA, Fink CL, Fry JS et al. 1983. Expression of bacterial genes in plant cells. *Proceedings of the National Academy of Sciences of the United States of America* **80**: 4803-4807.

Furuta KM, Hellmann E, Helariutta Y. 2014. Molecular control of cell specification and cell differentiation during procambial development. *Annual review of plant biology* **65**: 607-638.

Haseloff J, Siemering KR, Prasher DC, Hodge S. 1997. Removal of a cryptic intron and subcellular localization of green fluorescent protein are required to mark transgenic Arabidopsis plants brightly. *Proceedings of the National Academy of Sciences of the United States of America* **94**: 2122-2127.

Hazak O, Brandt B, Cattaneo P, Santiago J, Rodriguez-Villalon A, Hothorn M, Hardtke CS. 2017. Perception of root-active CLE peptides requires CORYNE function in the phloem vasculature. *EMBO reports* **18**: 1367-1381.

bioRxiv preprint doi: https://doi.org/10.1101/2019.12.21.885863; this version posted December 23, 2019. The copyright holder for this preprint (which was not certified by peer review) is the author/funder, who has granted bioRxiv a license to display the preprint in perpetuity. It is made available under aCC-BY-NC 4.0 International license.

Hellens RP, Edwards EA, Leyland NR, Bean S, Mullineaux PM. 2000. pGreen: a versatile and flexible binary Ti vector for Agrobacterium-mediated plant transformation. *Plant molecular biology* **42**: 819-832.

Jiang L, Liu X, Xiong G, Liu H, Chen F, Wang L, Meng X, Liu G, Yu H, Yuan Y et al. 2013. DWARF 53 acts as a repressor of strigolactone signalling in rice. *Nature* **504**: 401-405.

Kondo Y, Nurani AM, Saito C, Ichihashi Y, Saito M, Yamazaki K, Mitsuda N, Ohme-Takagi M, Fukuda H. 2016. Vascular Cell Induction Culture System Using Arabidopsis Leaves (VISUAL) Reveals the Sequential Differentiation of Sieve Element-like Cells. *Plant Cell* **28**: 1250-1262.

Krogan NT, Long JA. 2009. Why so repressed? Turning off transcription during plant growth and development. *Curr Opin Plant Biol* **12**: 628-636.

Kurihara D, Mizuta Y, Sato Y, Higashiyama T. 2015. ClearSee: a rapid optical clearing reagent for whole-plant fluorescence imaging. *Development (Cambridge, England)* **142**: 4168-4179.

Ladwig F, Dahlke RI, Stuhrwohldt N, Hartmann J, Harter K, Sauter M. 2015. Phytosulfokine Regulates Growth in Arabidopsis through a Response Module at the Plasma Membrane That Includes CYCLIC NUCLEOTIDE-GATED CHANNEL17, H+-ATPase, and BAK1. *Plant Cell* **27**: 1718-1729.

Lampropoulos A, Sutikovic Z, Wenzl C, Maegele I, Lohmann JU, Forner J. 2013. GreenGate---a novel, versatile, and efficient cloning system for plant transgenesis. *PloS one* **8**: e83043.

Legrain P, Wojcik J, Gauthier JM. 2001. Protein--protein interaction maps: a lead towards cellular functions. *Trends Genet* **17**: 346-352.

Liang Y, Ward S, Li P, Bennett T, Leyser O. 2016. SMAX1-LIKE7 Signals from the Nucleus to Regulate Shoot Development in Arabidopsis via Partially EAR Motif-Independent Mechanisms. *Plant Cell* **28**: 1581-1601.

Lin TF, Saiga S, Abe M, Laux T. 2016. OBE3 and WUS Interaction in Shoot Meristem Stem Cell Regulation. *PloS one* **11**: e0155657.

Lucas WJ, Groover A, Lichtenberger R, Furuta K, Yadav SR, Helariutta Y, He XQ, Fukuda H, Kang J, Brady SM et al. 2013. The plant vascular system: evolution, development and functions. *Journal of integrative plant biology* **55**: 294-388.

Ma H, Duan J, Ke J, He Y, Gu X, Xu TH, Yu H, Wang Y, Brunzelle JS, Jiang Y et al. 2017. A D53 repression motif induces oligomerization of TOPLESS corepressors and promotes assembly of a corepressor-nucleosome complex. *Science advances* **3**: e1601217.

Marhava P, Aliaga Fandino AC, Koh SWH, Jelinkova A, Kolb M, Janacek DP, Breda AS, Cattaneo P, Hammes UZ, Petrasek J et al. 2019. Plasma membrane domain patterning and self-reinforcing polarity in Arabidopsis. *Developmental cell*.

Marhava P, Bassukas AEL, Zourelidou M, Kolb M, Moret B, Fastner A, Schulze WX, Cattaneo P, Hammes UZ, Schwechheimer C et al. 2018. A molecular rheostat adjusts auxin flux to promote root protophloem differentiation. *Nature* **558**: 297-300.

Oparka KJ, Turgeon R. 1999. Sieve elements and companion cells-traffic control centers of the phloem. *Plant Cell* **11**: 739-750.

Pauwels L, Barbero GF, Geerinck J, Tilleman S, Grunewald W, Perez AC, Chico JM, Bossche RV, Sewell J, Gil E et al. 2010. NINJA connects the co-repressor TOPLESS to jasmonate signalling. *Nature* **464**: 788-791.

Rodriguez-Villalon A. 2016. Wiring a plant: genetic networks for phloem formation in Arabidopsis thaliana roots. *New Phytol* **210**: 45-50.

Rodriguez-Villalon A, Gujas B, Kang YH, Breda AS, Cattaneo P, Depuydt S, Hardtke CS. 2014. Molecular genetic framework for protophloem formation. *Proceedings of the National Academy of Sciences of the United States of America* **111**: 11551-11556.

Rodriguez-Villalon A, Gujas B, van Wijk R, Munnik T, Hardtke CS. 2015. Primary root protophloem differentiation requires balanced phosphatidylinositol-4,5-biphosphate levels and systemically affects root branching. *Development (Cambridge, England)* **142**: 1437-1446.

bioRxiv preprint doi: https://doi.org/10.1101/2019.12.21.885863; this version posted December 23, 2019. The copyright holder for this preprint (which was not certified by peer review) is the author/funder, who has granted bioRxiv a license to display the preprint in perpetuity. It is made available under aCC-BY-NC 4.0 International license.

Ross-Elliott TJ, Jensen KH, Haaning KS, Wager BM, Knoblauch J, Howell AH, Mullendore DL, Monteith AG, Paultre D, Yan D et al. 2017. Phloem unloading in Arabidopsis roots is convective and regulated by the phloem-pole pericycle. *Elife* **6**: e24125.

Saiga S, Furumizu C, Yokoyama R, Kurata T, Sato S, Kato T, Tabata S, Suzuki M, Komeda Y. 2008. The Arabidopsis OBERON1 and OBERON2 genes encode plant homeodomain finger proteins and are required for apical meristem maintenance. *Development (Cambridge, England)* **135**: 1751-1759.

Saiga S, Moller B, Watanabe-Taneda A, Abe M, Weijers D, Komeda Y. 2012. Control of embryonic meristem initiation in Arabidopsis by PHD-finger protein complexes. *Development (Cambridge, England)* **139**: 1391-1398.

Sanchez R, Zhou MM. 2011. The PHD finger: a versatile epigenome reader. *Trends Biochem Sci* **36**: 364-372.

Scacchi E, Salinas P, Gujas B, Santuari L, Krogan N, Ragni L, Berleth T, Hardtke CS. 2010. Spatio-temporal sequence of cross-regulatory events in root meristem growth. *Proceedings of the National Academy of Sciences of the United States of America* **107**: 22734-22739.

Schindelin J, Arganda-Carreras I, Frise E, Kaynig V, Longair M, Pietzsch T, Preibisch S, Rueden C, Saalfeld S, Schmid B et al. 2012. Fiji: an open-source platform for biological-image analysis. *Nat Methods* **9**: 676-682.

Scholthof HB. 2006. The Tombusvirus-encoded P19: from irrelevance to elegance. *Nat Rev Microbiol* **4**: 405-411.

Schwab R, Ossowski S, Riester M, Warthmann N, Weigel D. 2006. Highly Specific Gene Silencing by Artificial MicroRNAs in Arabidopsis. *Plant Cell* **18**: 1121-1133.

Soundappan I, Bennett T, Morffy N, Liang Y, Stanga JP, Abbas A, Leyser O, Nelson DC. 2015. SMAX1-LIKE/D53 family members enable distinct MAX2-dependent responses to strigolactones and karrikins in Arabidopsis. *Plant Cell* **27**: 3143-3159.

Stanga JP, Morffy N, Nelson DC. 2016. Functional redundancy in the control of seedling growth by the karrikin signaling pathway. *Planta* **243**: 1397-1406.

Stanga JP, Smith SM, Briggs WR, Nelson DC. 2013. SUPPRESSOR OF MORE AXILLARY GROWTH2 1 controls seed germination and seedling development in Arabidopsis. *Plant physiology* **163**: 318-330.

Thomas CL, Schmidt D, Bayer EM, Dreos R, Maule AJ. 2009. Arabidopsis plant homeodomain finger proteins operate downstream of auxin accumulation in specifying the vasculature and primary root meristem. *The Plant journal : for cell and molecular biology* **59**: 426-436.

Truernit E, Bauby H, Belcram K, Barthelemy J, Palauqui JC. 2012. OCTOPUS, a polarly localised membrane-associated protein, regulates phloem differentiation entry in Arabidopsis thaliana. *Development (Cambridge, England)* **139**: 1306-1315.

Truernit E, Bauby H, Dubreucq B, Grandjean O, Runions J, Barthelemy J, Palauqui JC. 2008. High-resolution whole-mount imaging of three-dimensional tissue organization and gene expression enables the study of Phloem development and structure in Arabidopsis. *Plant Cell* **20**: 1494-1503.

van den Berg C, Willemsen V, Hendriks G, Weisbeek P, Scheres B. 1997. Short-range control of cell differentiation in the Arabidopsis root meristem. *Nature* **390**: 287-289.

Voinnet O, Rivas S, Mestre P, Baulcombe D. 2003. An enhanced transient expression system in plants based on suppression of gene silencing by the p19 protein of tomato bushy stunt virus. *The Plant journal : for cell and molecular biology* **33**: 949-956.

Walker C, Bennett T. 2017. Reassessing the evolution of strigolactone synthesis and signalling. *bioRxiv*: 228320.

Wallner ES. 2018. Early events in phloem formation: Exploring the molecular network of SMXL3/4/5. in *Faculty for Biosiences*, p. 128. University of Heidelberg, Heidelberg.

Wallner ES, Lopez-Salmeron V, Belevich I, Poschet G, Jung I, Grunwald K, Sevilem I, Jokitalo E, Hell R, Helariutta Y et al. 2017. Strigolactone- and Karrikin-Independent SMXL Proteins Are Central Regulators of Phloem Formation. *Current biology : CB* **27**: 1241-1247.

bioRxiv preprint doi: https://doi.org/10.1101/2019.12.21.885863; this version posted December 23, 2019. The copyright holder for this preprint (which was not certified by peer review) is the author/funder, who has granted bioRxiv a license to display the preprint in perpetuity. It is made available under aCC-BY-NC 4.0 International license.

Wallner ES, Lopez-Salmeron V, Greb T. 2016. Strigolactone versus gibberellin signaling: reemerging concepts? *Planta* **243**: 1339-1350.

Wallner ES, Tonn N, Shi D, Jouannet V, Greb T. 2020. SUPPRESSOR OF MAX2 1-LIKE 5 promotes secondary phloem formation during radial stem growth. *The Plant journal : for cell and molecular biology* **in press**.

Wang L, Wang B, Jiang L, Liu X, Li X, Lu Z, Meng X, Wang Y, Smith SM, Li J. 2015. Strigolactone signaling in Arabidopsis regulates shoot development by targeting D53-Like SMXL repressor proteins for ubiquitination and degradation. *Plant Cell* **27**: 3128-3142.

Wu YY, Hou BH, Lee WC, Lu SH, Yang CJ, Vaucheret H, Chen HM. 2017. DCL2- and RDR6-dependent transitive silencing of SMXL4 and SMXL5 in Arabidopsis dcl4 mutants causes defective phloem transport and carbohydrate over-accumulation. *The Plant journal : for cell and molecular biology* **90**: 1064-1078.

Zhou F, Lin Q, Zhu L, Ren Y, Zhou K, Shabek N, Wu F, Mao H, Dong W, Gan L et al. 2013. D14-SCF(D3)-dependent degradation of D53 regulates strigolactone signalling. *Nature* **504**: 406-410.

bioRxiv preprint doi: https://doi.org/10.1101/2019.12.21.885863; this version posted December 23, 2019. The copyright holder for this preprint (which was not certified by peer review) is the author/funder, who has granted bioRxiv a license to display the preprint in perpetuity. It is made available under aCC-BY-NC 4.0 International license.

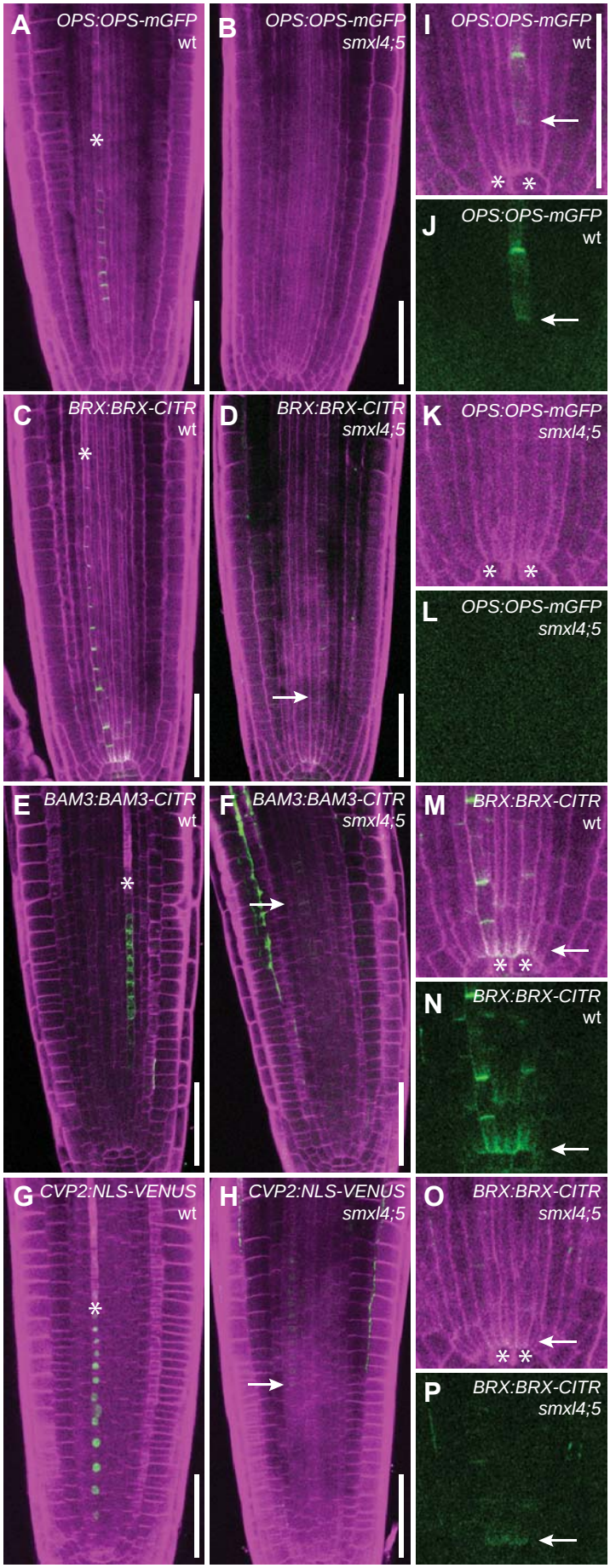

Figure 1: Phloem-related genes are less active in *smxl4;smxl5* mutants
(A – H) Comparison of *OPS:OPS-GFP* (A, B), *BRX:BRX-CITRINE* (C, D), *BAM3:BAM3-CITRINE*, and *CVP2:NLS-VENUS* (G, H) reporter activities in wild type (A, C, E, G) and *smxl4;smxl5* double mutants (B, D, F, H). Asterisks depict the first differentiating SE. Arrows point to earliest detectable reporter activities. Scale bars represent 50 µm.
(I – P) *OPS:OPS-GFP* (I-L) and *BRX-:BRX-CITRINE* (M-P) close to the QC in wild type (I, J, M, N) and *smxl4;smxl5* mutants (K, L, O, P). In J, L, N, and P, fluorescent signals are depicted without counterstaining. Asterisks indicate QC cells. Arrows point to earliest detectable reporter activities. Scale bar in (I) represents 50 µm. Same magnification in I-P.

bioRxiv preprint doi: https://doi.org/10.1101/2019.12.21.885863; this version posted December 23, 2019. The copyright holder for this preprint (which was not certified by peer review) is the author/funder, who has granted bioRxiv a license to display the preprint in perpetuity. It is made available under aCC-BY-NC 4.0 International license.

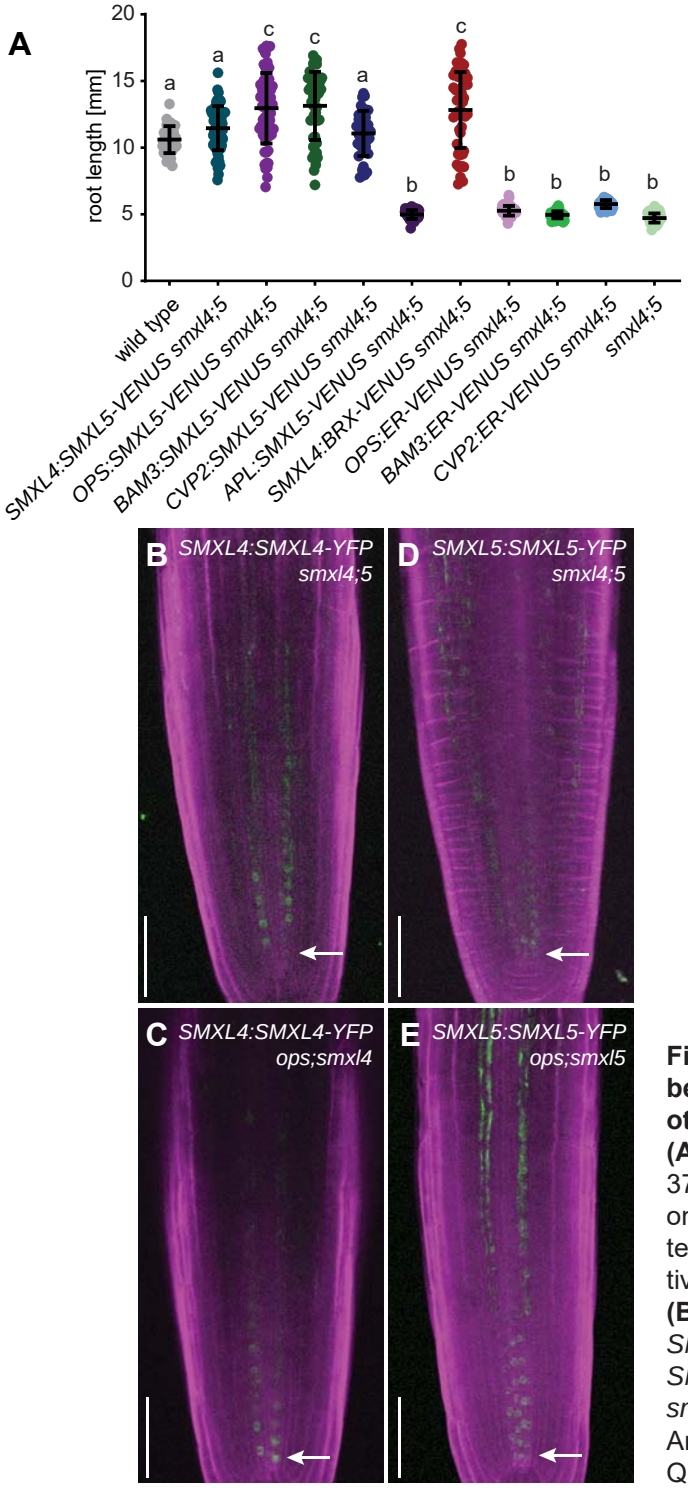

Figure 2 : Analysis of interaction between *SMXL4* and *SMXL5* with other phloem regulators

(A) Root length of five day-old plants. n = 37–75. Statistical groups determined by one-way ANOVA and post-hoc Tukey's test (95 % CI). Shown is one representative experiment of three repetitions.

(B – E) Comparison of *SMXL4:SMXL4-YFP* and *SMXL5:SMXL5-YFP* reporter activities in *smxl4;smxl5* and *smxl;ops* mutants. Arrows indicate the signals closest to the QC. Scale bars represent 50 µm.

bioRxiv preprint doi: https://doi.org/10.1101/2019.12.21.885863; this version posted December 23, 2019. The copyright holder for this preprint (which was not certified by peer review) is the author/funder, who has granted bioRxiv a license to display the preprint in perpetuity. It is made available under aCC-BY-NC 4.0 International license.

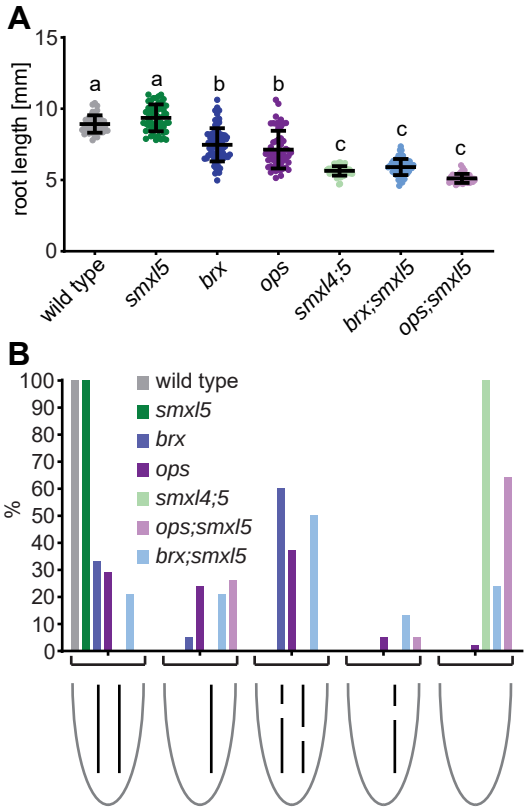

Figure 3: Genetic interaction of *SMXL5* with *OPS* and *BRX*

(A) Root length of five day-old wild type (WT), *smxl5*, *brx*, *ops*, *smxl4;smxl5*, *brx;smxl5*, and *ops;smxl5* plants. n = 38–76 for ech group. Statistical groups determined by one-way ANOVA and post-hoc Tukey's HSD test (95 % CI). Shown is one representative experiment of three repetitions.

(B) Phenotypic characterization of phloem development of two day-old wild type, *smxl5*, *brx*, *ops*, *smxl4;smxl5*, *brx;smxl5*, and *ops;smxl5* plants. n = 97–129 for each group.

bioRxiv preprint doi: https://doi.org/10.1101/2019.12.21.885863; this version posted December 23, 2019. The copyright holder for this preprint (which was not certified by peer review) is the author/funder, who has granted bioRxiv a license to display the preprint in perpetuity. It is made available under aCC-BY-NC 4.0 International license.

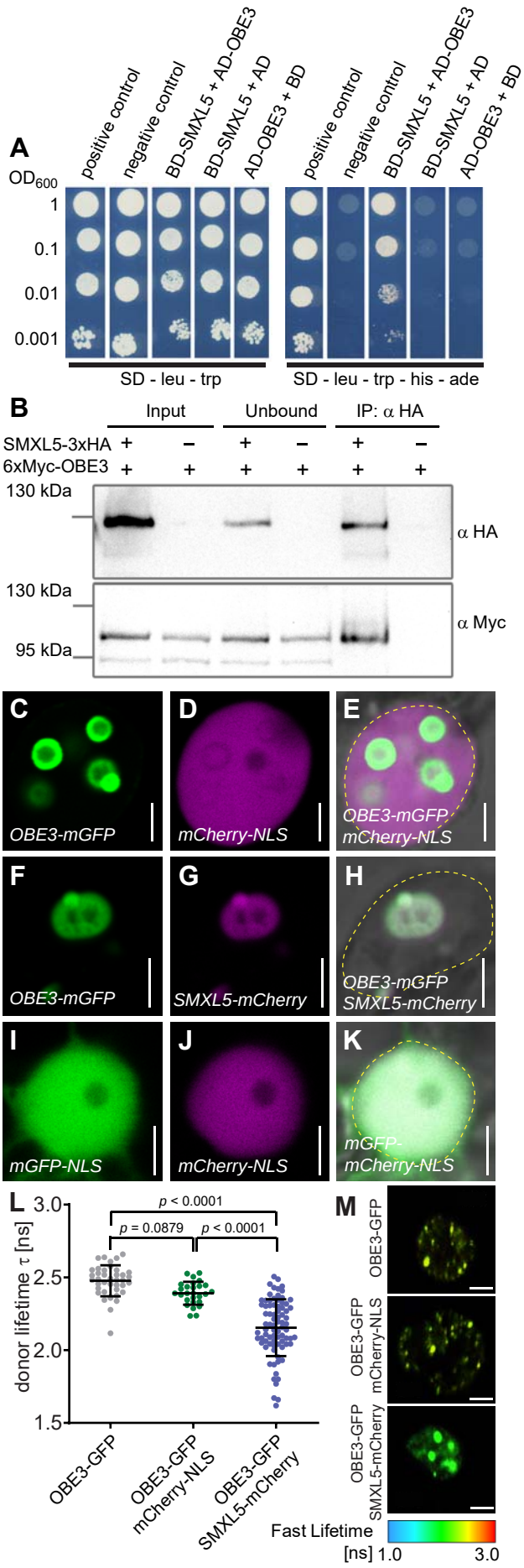

Figure 4: SMXL5 and OBE3 proteins interact

(A) The SMXL5 protein was expressed in yeast fused to the GAL4 DNA binding domain (BD) and OBE3 fused to the GAL4 activation domain (AD). All strains contained AD- and BD-expressing plasmids either alone or fused with SMXL5, OBE3 or control proteins, respectively. Growth on SD-leu-trp indicate the presence of both plasmids, growth on SD-leu-trp-his-ade medium indicate the presence of plasmids and protein interaction.

(B) Interaction of SMXL5-3xHA and 6xMyc-OBE3 proteins by co-immunoprecipitation (co-IP) and subsequent Western blot analysis after transient overexpression in *N. benthamiana*. 'Input' represents unprocessed protein extracts, 'unbound' show proteins that remained in the extract after IP and 'IP: α HA' depicts samples after immunoprecipitation by α-HA-beads. Western blots were probed by α HA or α Myc antibodies, respectively. Signals revealed an expected SMXL5-3xHA protein size of approximately 120 kDa. The size of the detected 6xMyc-OBE3 protein (~100 kDa) exceeded the expected size of 92 kDa.

(C – K) Fluorescent signals and bright field images of epidermal *N. benthamiana* nuclei transiently co-expressing OBE3-mGFP/mCherry (C-E), OBE3-mGFP/SMXL5-mCherry (F-H) and mGFP-NLS/mCherry-NLS (I-K). The dashed yellow line indicates the outlines of nuclei in merged images (E, H, K). Scale bars represent 5 µm.

(L) FRET-FLIM analysis of transiently transformed *N. benthamiana* epidermal leaf cells expressing the OBE3-mGFP donor in the presence of SMXL5-mCherry or NLS-mCherry or without an mCherry acceptor. Error bars indicate standard deviation. P-values for lifetime comparisons are based on Dunn post hoc analysis following a Wilcoxon / Kruskal-Wallis test. Data were derived from three biological replicates with n = 27–80. To test for homogeneity of variance, a Brown-Forsythe test was applied. As the variances are not homogenous a Wilcoxon / Kruskal-Wallis test was carried out followed by a Dunn post hoc analysis.

(M) Heat maps of representative nuclei used for FLIM measurements. The donor lifetimes of OBE3-mGFP are color-coded according to the scale at the bottom. Size bars represent 4 µm.

bioRxiv preprint doi: https://doi.org/10.1101/2019.12.21.885863; this version posted December 23, 2019. The copyright holder for this preprint (which was not certified by peer review) is the author/funder, who has granted bioRxiv a license to display the preprint in perpetuity. It is made available under aCC-BY-NC 4.0 International license.

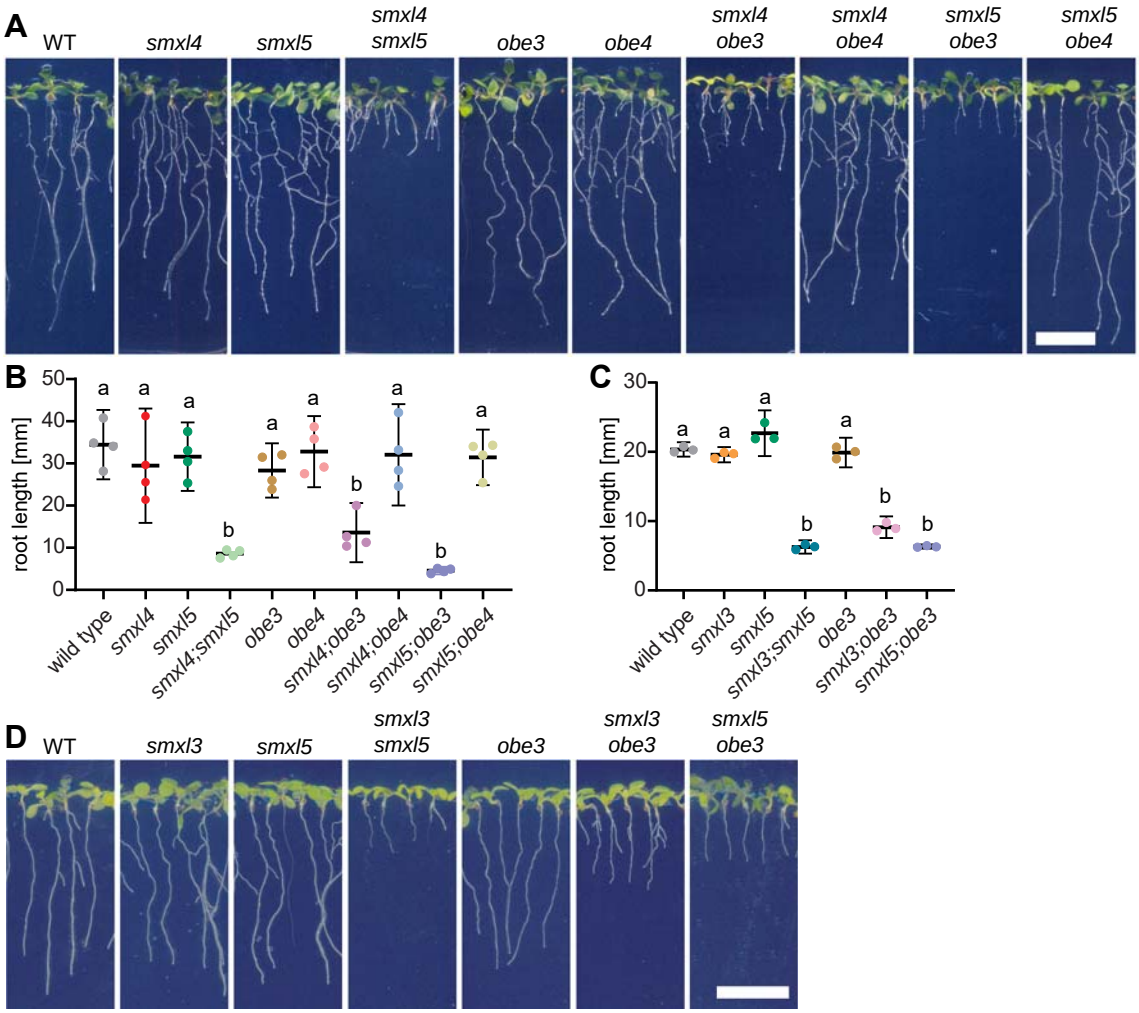

Figure 5: *OBE3* genetically interacts with *SMXL3/4/5* in root growth regulation

(A) 10 day-old wild type, *smxl4*, *smxl5*, *smxl4;smxl5*, *obe3*, *obe4*, *smxl4;obe3*, *smxl4;obe4*, *smxl5;obe3*, *smxl5;obe4* seedlings are shown from left to right. Scale bar represents 1 cm.

(B) Quantification of root length depicted in A. Mean values of four independent experiments (n = 15-55 per experiment and genotype) were analyzed by a one-way ANOVA with post-hoc Tukey HSD (95 % CI). Statistical groups are marked by letters.

(C) Quantification of root length depicted in D. Mean values of three independent experiments (n = 62–74 per experiment and genotype) were analyzed by a one-way ANOVA with post-hoc Tamhane-T2 (95 % CI). Statistical groups are marked by letters.

(D) 10 day-old wild type, *smxl3*, *smxl5*, *smxl3;smxl5*, *obe3*, *smxl3;obe3*, *smxl5;obe3* seedlings are shown from left to right. Scale bar represents 1 cm.

bioRxiv preprint doi: https://doi.org/10.1101/2019.12.21.885863; this version posted December 23, 2019. The copyright holder for this preprint (which was not certified by peer review) is the author/funder, who has granted bioRxiv a license to display the preprint in perpetuity. It is made available under aCC-BY-NC 4.0 International license.

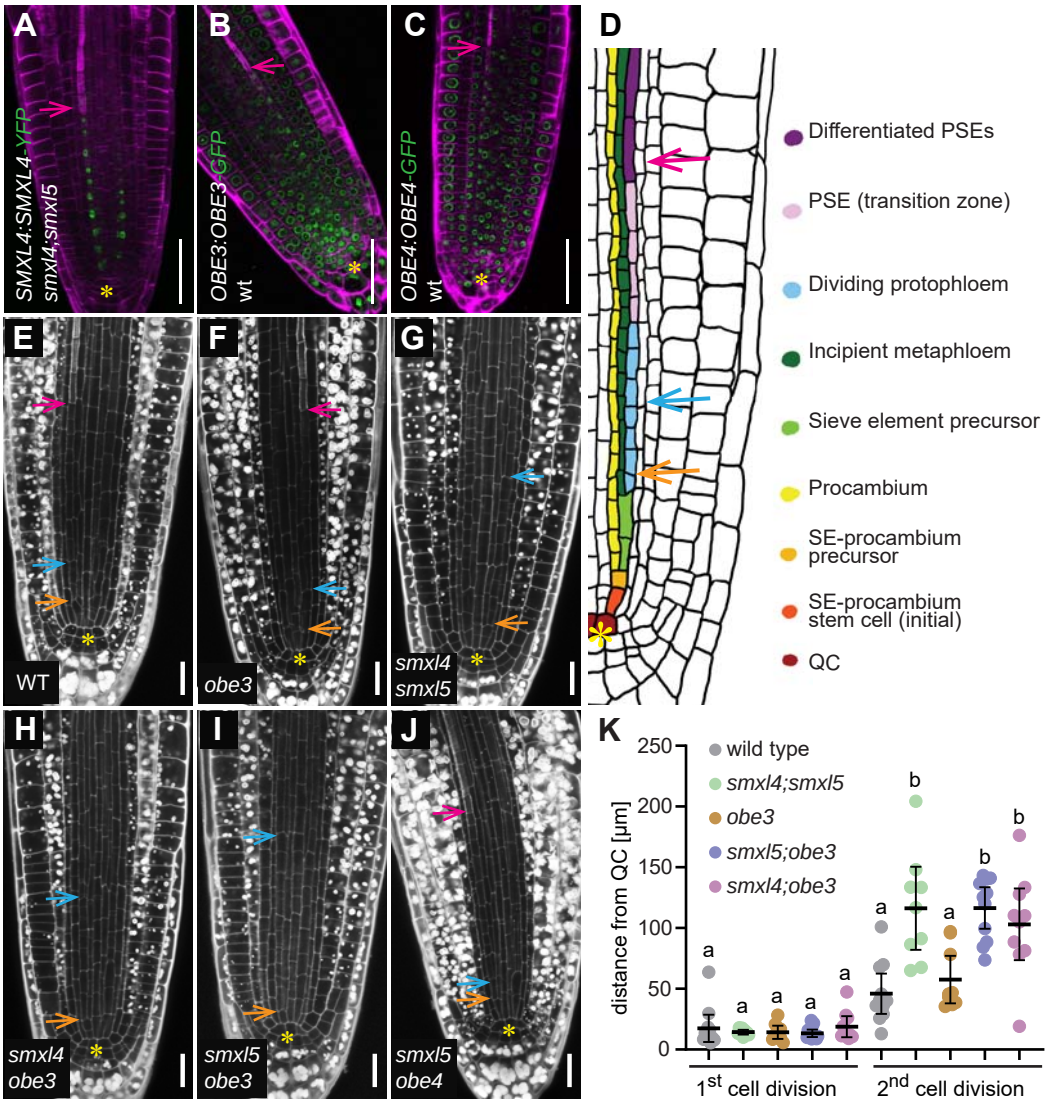

Figure 6: *OBE3* interacts with *SMXL5* during protophloem formation

(A – C) Phloem-specific activity of *SMXL4:SMXL4-YFP* (A) coincides with activty of *OBE3:OBE3-GFP* (B) and *OBE4:OBE4-GFP* (C) reporters in the developing phloem. Fluorescent signals (green) and cell wall staining by Direct Red 23 (magenta) were detected by confocal microscopy. Pink arrows point to the first differentiated SE indicated by enhanced cell wall staining. Scale bars represent 50 µm.

(D) Schematic representation of one developing phloem pole at the root tip. Two tangential cell divisions generate SE precursor and procambium (orange arrow) and proto- and metaphloem cell lineages (blue arrow), respectively. Differentiated SEs are marked by a pink arrow. The QC is marked by a yellow asterisk.

(E – J) Phloem formation in 2 day-old wild type (E), *obe3* (F), *smxl4;smxl5* (G), *smxl4;obe3* (H), *smxl5;obe3* (I) and *smxl5;obe4* (J) root tips. Cell walls were stained by mPS-PI (white). Yellow asterisks mark the QC. Enhanced mPS-PI staining indicates differentiation of SEs (pink arrows) in wild type (E), *obe3* (F) and *obe4;smxl5* (G). Orange and blue arrows mark the first and second tangential division, respectively, in the developing phloem cell lineage. Scale bars represent 20 µm.

(K) The distance from the QC to the first and second tangential division shown in D-I was quantified (n = 9–11). Statistical groups are indicated by letters and were determined by a one-way ANOVA with post-hoc Tukey HSD (95 % CI). Distances of 1st cell divisions and 2nd cell divisions were compared independently.

bioRxiv preprint doi: https://doi.org/10.1101/2019.12.21.885863; this version posted December 23, 2019. The copyright holder for this preprint (which was not certified by peer review) is the author/funder, who has granted bioRxiv a license to display the preprint in perpetuity. It is made available under aCC-BY-NC 4.0 International license.

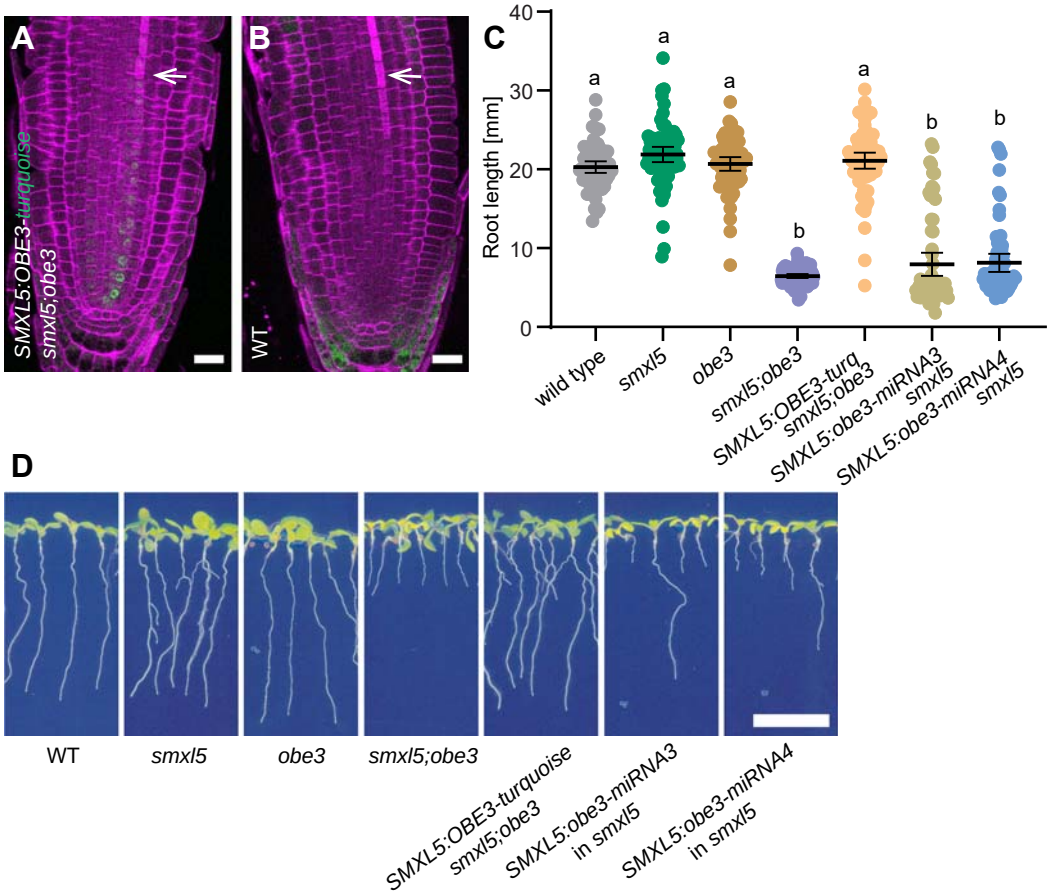

Figure 7: Phloem-specific *OBE3* expression is sufficient for promoting root growth

(A – B) Seven day-old *smxl5;obe3* root tips carrying an *SMXL5:OBE3-turquoise* reporter (green signal, B) were compared to a non-transformed wild type (WT) root tip (B). Cell walls were stained by DirectRed (magenta). White arrows mark differentiated SEs. Scale bars indicate 20 µm.

(C) Root length quantification of plants depicted in D. Results from one representative experiment out of three independent experiments (n = 61–71 per experiment and genotype) are shown. Mean values were analyzed by one-way ANOVA with post-hoc Tamhane-T2 (95 % CI). Statistical groups are indicated by letters.

(D) 10 day-old wild type, *smxl5*, *obe3*, *smxl5;obe3*, *SMXL5:OBE3-turquoise/smxl5;obe3*, *SMXL5:obe3-miRNA3/smxl5* and *SMXL5:obe3-miRNA4/smxl5* seedlings are shown from left to right. Scale bar represents 1 cm.

bioRxiv preprint doi: https://doi.org/10.1101/2019.12.21.885863; this version posted December 23, 2019. The copyright holder for this preprint (which was not certified by peer review) is the author/funder, who has granted bioRxiv a license to display the preprint in perpetuity. It is made available under aCC-BY-NC 4.0 International license.

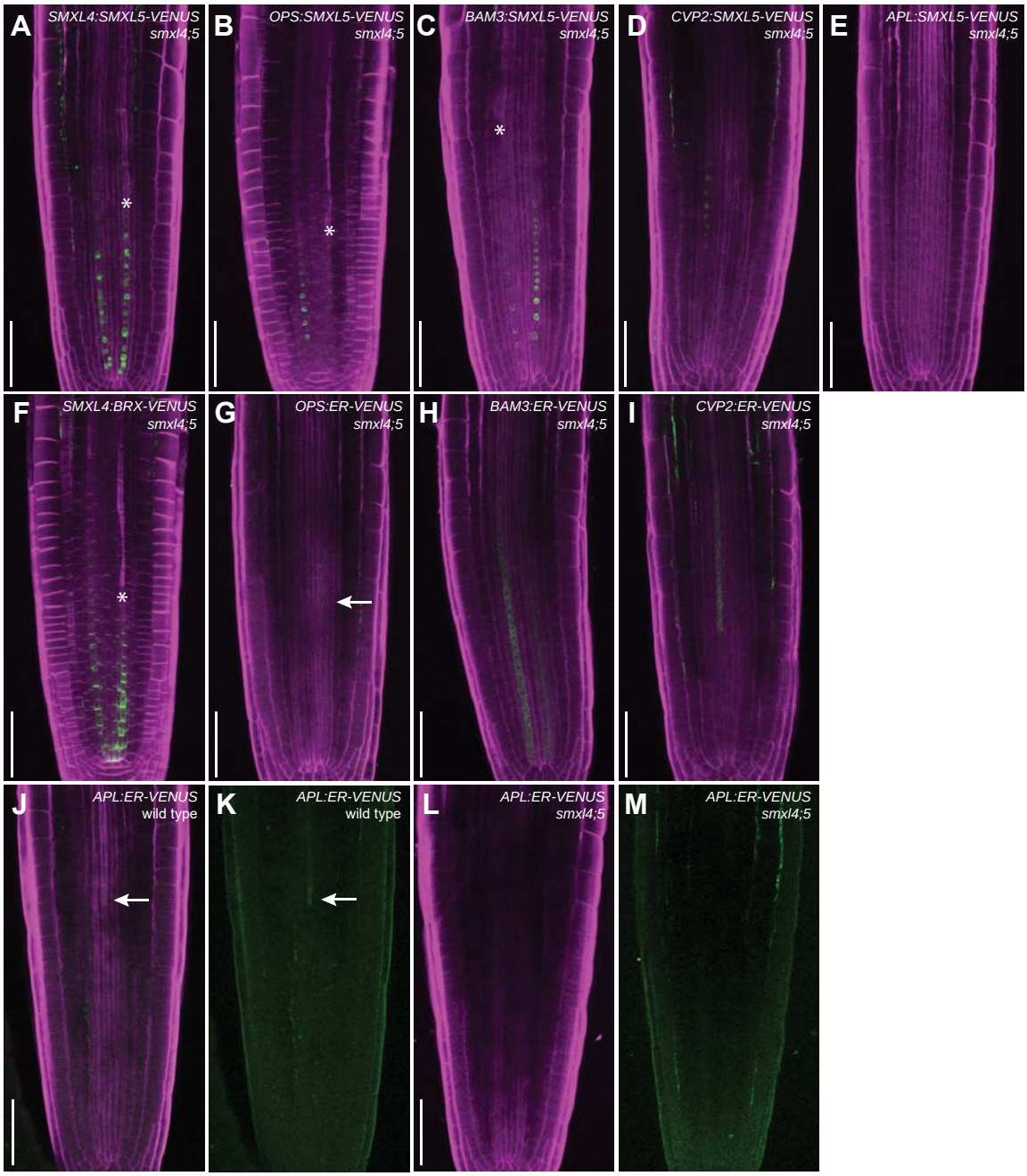

Supplementary Figure 1: Expression of SMXL5-VENUS protein fusions in *smxl4;smxl5* mutants in comparison to promoter reporters.

(A – E) Expression of SMXL5-VENUS protein fusions under the control of different heterologous promoters. Differentiated SEs are indicated by the asterisks.

(F) Detection of the BRX-VENUS protein fusion expressed under the control of the *SMXL4* promoter. Differentiated SEs are indicated by the asterisk.

(G – I) Detection of *OPS:ER-VENUS*, *BAM3:ER-VENUS*, and *CVP2:ER-VENUS* reporter activities in *smxl4;smxl5* mutants. Arrow in G points to a weakly detectable reporter-derived signal.

(J – M) Detection of *APL:ER-VENUS* reporter activity in wild type (J, K) and *smxl4;smxl5* mutants (L, M). K and M show the same root tip as in J and L, respectively, without the counter stain signal. Scale bars in all pictures represent 50 µm. Arrows in J and K point to a weakly detectable reporter-derived signal.

bioRxiv preprint doi: https://doi.org/10.1101/2019.12.21.885863; this version posted December 23, 2019. The copyright holder for this preprint (which was not certified by peer review) is the author/funder, who has granted bioRxiv a license to display the preprint in perpetuity. It is made available under aCC-BY-NC 4.0 International license.

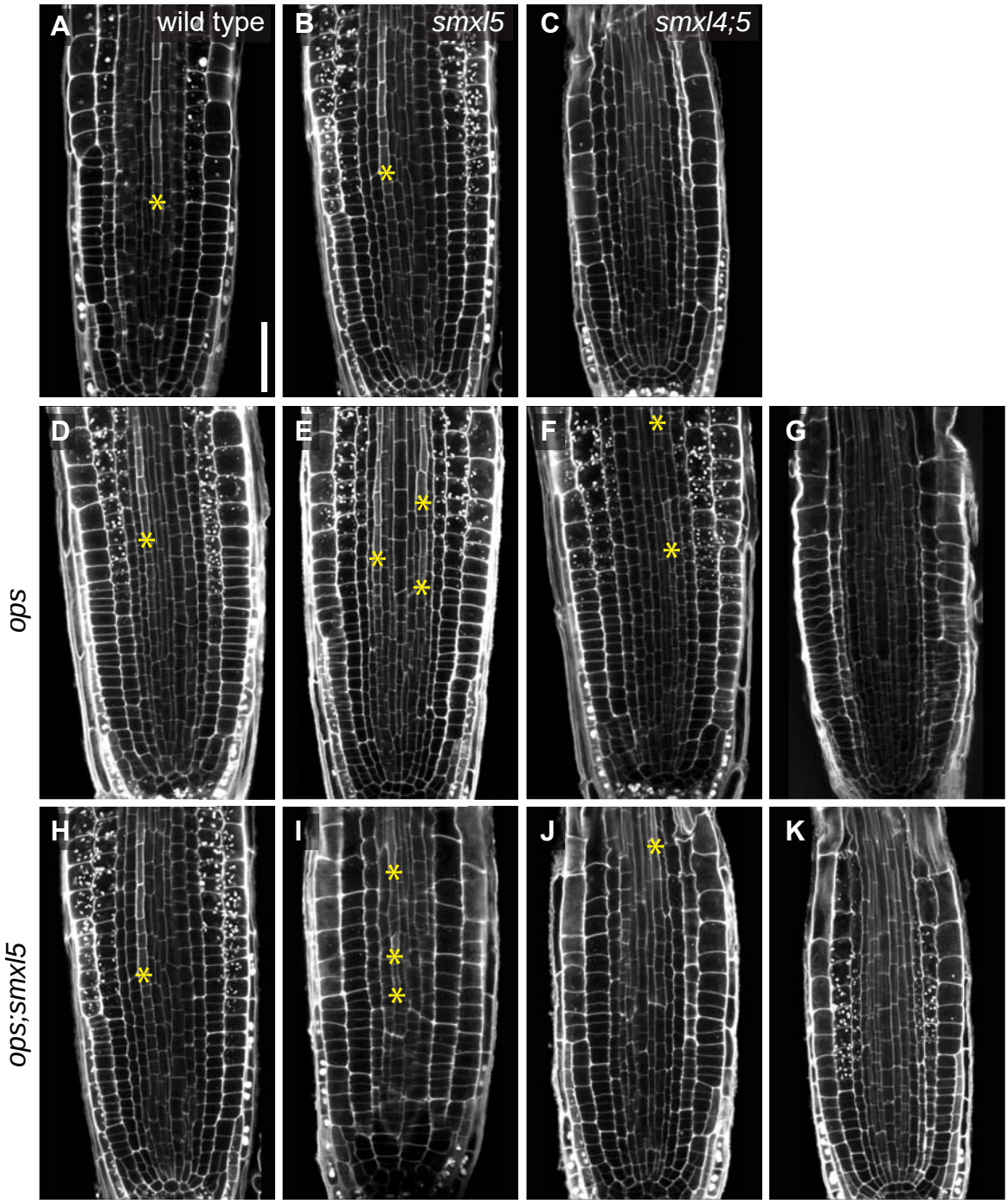

Supplementary Figure 2: Characterization of phloem development in *smxl* and *ops* mutants.
(A – K) Phloem development is monitored in wild type (A), *smxl5* (B), *smxl4;smxl5* (C), *ops* (D-G) and *ops;smxl5* (H-K) mutant backgrounds by confocal analysis of mPS-PI-stained root tips. Asterisks indicate the most apical appearance of differentiated SEs. In case 'gaps' are observed, more than one asterisk is depicted.

bioRxiv preprint doi: https://doi.org/10.1101/2019.12.21.885863; this version posted December 23, 2019. The copyright holder for this preprint (which was not certified by peer review) is the author/funder, who has granted bioRxiv a license to display the preprint in perpetuity. It is made available under aCC-BY-NC 4.0 International license.

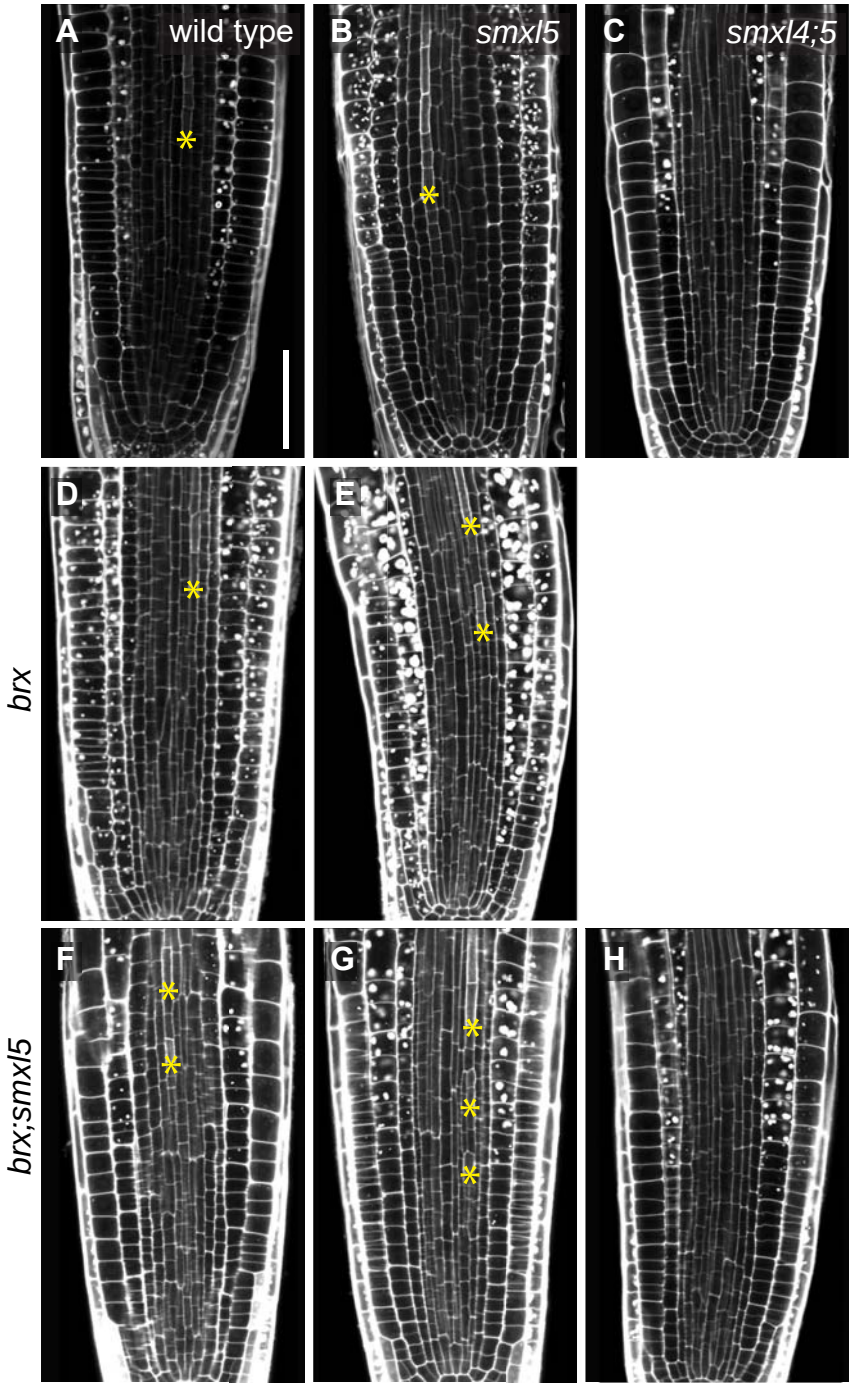

Supplementary Figure 3: Characterization of phloem development in *smxl* and *brx* mutants.
(A – H) Phloem development is monitored in wild type (A), *smxl5* (B), *smxl4;smxl5* (C), *brx* (D-E) and *brx;smxl5* (F-H) mutant backgrounds by confocal analysis of mPS-PI-stained root tips. Asterisks indicate the most apical appearance of differentiated SEs. In case 'gaps' are observed, more than one asterisk is depicted.

bioRxiv preprint doi: https://doi.org/10.1101/2019.12.21.885863; this version posted December 23, 2019. The copyright holder for this preprint (which was not certified by peer review) is the author/funder, who has granted bioRxiv a license to display the preprint in perpetuity. It is made available under aCC-BY-NC 4.0 International license.

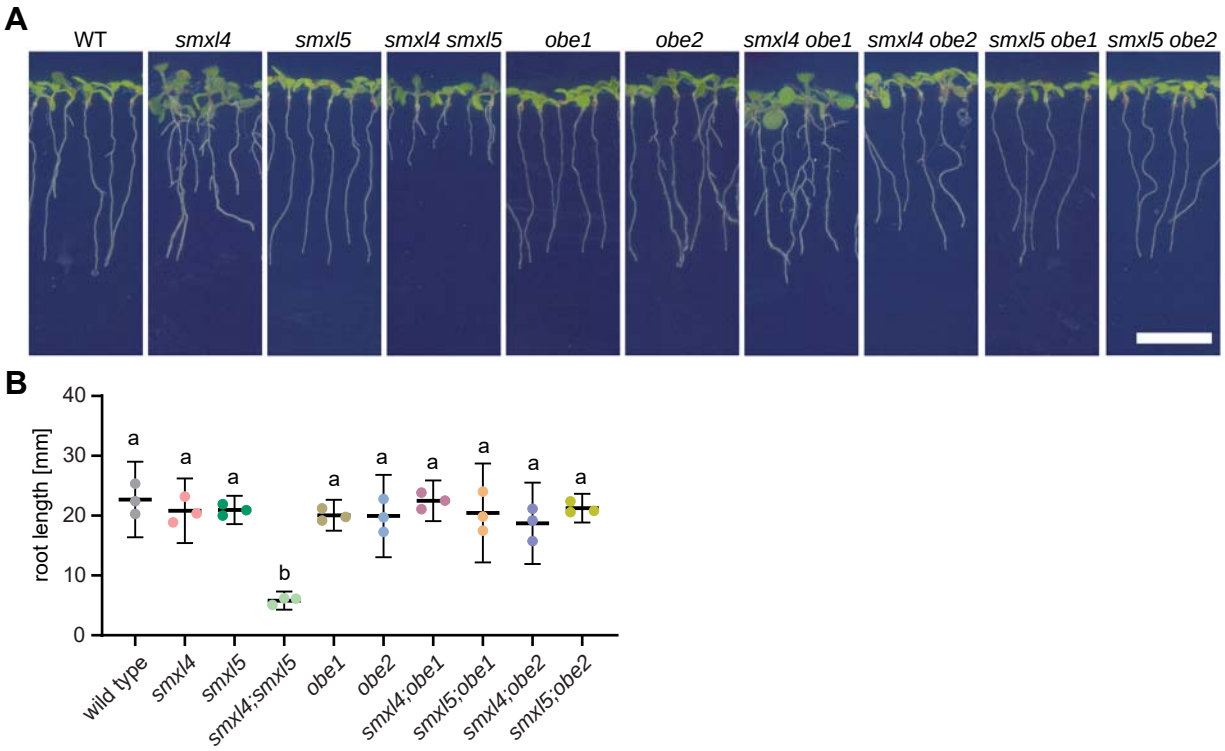

Supplementary Figure 4: *SMXL4* or *SMXL5* genes do not genetically interact with *OBE1* or *OBE2* genes
(A) 10 day-old wild type, *smxl4*, *smxl5*, *smxl4;smxl5*, *obe1*, *obe2*, *smxl4;obe1*, *smxl4;obe2*, *smxl5;obe1*, *smxl5;obe2* seedlings are shown from left to right. Scale bar represents 1 cm.
(B) Quantification of root lengths depicted in A. Mean values of three independent experiments (n = 34-75 per experiment and genotype) were analyzed by a one-way ANOVA with post-hoc Tukey HSD (95 % CI). Statistical groups are indicated by letters.

bioRxiv preprint doi: https://doi.org/10.1101/2019.12.21.885863; this version posted December 23, 2019. The copyright holder for this preprint (which was not certified by peer review) is the author/funder, who has granted bioRxiv a license to display the preprint in perpetuity. It is made available under aCC-BY-NC 4.0 International license.

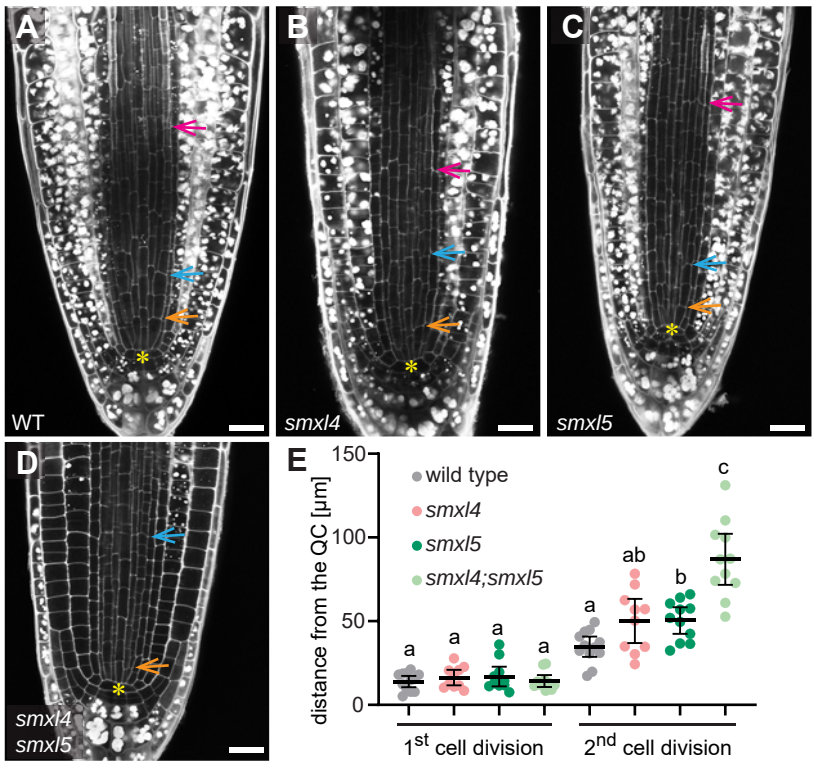

Supplementary Figure 5: SEs form in *smxl4* and *smxl5* single mutants

(A – D) 2 day-old mPS-PI-stained root tips of wild type (A), *smxl4* (B), *smxl5* (C) and *smxl4;smxl5* (D) plants. Differentiating SEs were observed in wild type, *smxl4* and *smxl5* (pink arrows). Tangential cell divisions are marked by orange and blue arrows. The QC is indicated by a yellow asterisk. Scale bars represent 20 µm.

(E) The distance of the first and second tangential division from the QC for plants shown in A-D was quantified (n = 10-12). Statistical groups marked by letters were determined by one-way ANOVA with post-hoc Tamhane-T2 (95 % CI). Distances of 1st cell divisions and 2nd cell divisions were compared independently.

bioRxiv preprint doi: https://doi.org/10.1101/2019.12.21.885863; this version posted December 23, 2019. The copyright holder for this preprint (which was not certified by peer review) is the author/funder, who has granted bioRxiv a license to display the preprint in perpetuity. It is made available under aCC-BY-NC 4.0 International license.

Supplementary Table 1: Oligonucleotides used in this study

	Used for	Primer name	Primer sequence (5' → 3')
Genotyping	*smxl3-1*	*SALK_024706_LP*	CCCTACACAGCTCTTCACGAG
		SALK_024706_RP	TGCCTCTCTCACAAGAAAAGC
	smxl4-1	*SALK_037136-LP*	TTGAAGCCATGGAAGAATCTG
		SALK_037136-RP	ACAAAGAACAATGCGGTCAAG
	smxl5-1	*SALK_018522-LP*	TGTCTCATTGAAGCCAAAACC
		SALK_018522-RP	AATGGTGCAAGAATTCTGACG
	obe1-1	*SALK_075710_LP*	ATTCGACTCAAACGTTGAACG
		SALK_075710_RP	CTCGTCTGGACAAACTTCTGC
	obe2-1	*obe2-1_RP*	CTTCAAGATCAAGGTATTGACCTAAATTACC
		obe2-1_LP	CATTTGGTGAGGATGATTCGAACC
		obe2-1_Insertion	GATCAGATTGTCGTTTCCCGCC
	obe3-1	*SALK_042597_LP*	TTCCAACAACAAAGGCTTTTG
		SALK_042597_RP	TTTCCCACAAAACGAAACAAG
	obe4-1	*SALK_082338_LP*	TGCTTATTGACACCTGACTGC
		SALK_082338_RP	AAGAAAAGCGAGGAGGAAGTG
		ops_RP	TCTTCCTCTAAAAAGCCTCCG
		ops_LP	CACACCGTTGGTTTGGTTAAC
	SALK_insert	*SALK_LBa1*	TGGTTCACGTAGTGGGCCATCG
	brx-2	*brx-2_RP*	GTCAGTGTTTGCTTCCTCTCTATG
		brx-2_LP	TATTTCCTTGTCTAGGTAAGAATCC
		brx-2_Insertion	TGATCCATGTAGATTTCCCGGACATGAA
Conventional cloning	*pEW31*	3xHA_for	ACTAGGATCCTCCGCTTCCTCCTGCGTAGTCCGGGACATCATAC
		3xHA_rev	ACTAAAGCTTATGTATCCTTATGATGTACCTGATTATG
	pEW33	3xHA_SMXL5_for	ACTAGGATCCAGGAGGAAGTGGAGGAAGTTATCCTTATGATGTAC CTG
		3xHA_SMXL5_rev	ACTACCCGGGTCATGCGTAGTCCGGGACATC
	miRNA PCRs for *pEW45/46*	P-0950 Oligo A	AACAGGTCTCAAACACTGCAGCCCCAAACACACGC
		P-0951 Oligo B	AACAGGTCTCTGCAGCCCCATGGCGATGCC
	pEW45	I_miRNAsOBE3_3	GATAATTTCTGGTATTGACTCAGTCTCTCTTTTGTATTCC
		II_miRNAaOBE3_3	GACTGAGTCAATACCAGAAATTATCAAAGAGAATCAATGA
		III_miRNA*sOBE3_3	GACTAAGTCAATACCTGAAATTTTCACAGGTCGTGATATG
		IV_miRNA*aOBE3_3	GAAAATTTCAGGTATTGACTTAGTCTACATATATATTCCT
	pEW46	I_miRNAsOBE3_4	GATAATTTCTGGTATTGACTCATTCTCTCTTTTGTATTCC
		II_miRNAaOBE3_4	GAATGAGTCAATACCAGAAATTATCAAAGAGAATCAATGA
		III_miRNA*sOBE3_4	GAATAAGTCAATACCTGAAATTTTCACAGGTCGTGATATG
		IV_miRNA*aOBE3_4	GAAAATTTCAGGTATTGACTTATTCTACATATATATTCCT
GreenGate Cloning	*pNT51*	pOPS-for	AACAGGTCTCAACCTCAATGATGAATTATACTTACGTGGG
		pOPS-rev	AACAGGTCTCATGTTGACGGGAAATGGTGGTTAATC
	pVL84	SMXL5_GG1	AACAGGTCTCAGGCTCAATGCGAACAGGTGGTTATACG
		SMXL5_GG2	AACAGGTCTCACTGACTCCTCGAACTTGGAAACTTG
	pNT48	pBAM3-for	AACAGGTCTCAACCTGGTGGTTGGAGATG
		pBAM3-rev	AACAGGTCTCATGTTTGTAACATCAGAAAAATAAAAAC
	pNT9	pCVP2_FOR	AACA GGTCTC A ACCT CACAACTACCTAACTGATG
		pCVP2_REV	AACA GGTCTC A TGTT TGTTGCTTCTTCTCTGCAAG
	pNT42	pSMXL4-for	AACAGGTCTCAACCTACCATGTCGAACCCTCCAATTG
		pSMXL4-rev	AACAGGTCTCATGTTCACAAAACCACCCACCTTAAATC
	pNT71	BRX CDS for	AACAGGTCTCAGGCTCAATGTTTTCTTGCATAGCTTG
		BRX CDS rev	AACAGGTCTCACTGAGAGGTACTGTGTTTGTATTCTC
	pVL85	OBE3_GG1	AACAGGTCTCAGGCTCAATGATCGGAGAGAAAGATC
		OBE3_GG3	AACAGGTCTCACTGATCCTACCAATTGTTGTCTTG
	pEW75	cMyc_ModulB_for	AACAGGTCTCAAACAATGGAGCAAAAGCTC
		cMyc_ModulB_rev	AACAGGTCTCAAGCCCAAGTCCTCTTCAGA
	pCW192	A02603	AGTGAAGCTTGGTCTCAAACAATGGTGAGCAAGGGCGA
		A03062	GTTAGGTCTCAAGCCGGACTTGTACAGCTCGTCCATG

bioRxiv preprint doi: https://doi.org/10.1101/2019.12.21.885863; this version posted December 23, 2019. The copyright holder for this preprint (which was not certified by peer review) is the author/funder, who has granted bioRxiv a license to display the preprint in perpetuity. It is made available under aCC-BY-NC 4.0 International license.

	pCW193	A03064	GCTTGGTCTCAGGCTCTGGATCTATGGTGAGCAAGGGCGAGGA
		A02531	AACAGGTCTCACTGACTTGTACAGCTCGTCCATG

Supplementary Table 2: Destination modules created by GreenGate cloning (this study)

List of destination modules (GreenGate Cloning)							
Final construct (name)	Entry modules (list)						
	A	B	C	D	E	F	Z
OPS:SMXL5-VENUS (pNT52)	*pNT51*	*pVL50*	*pVL84*	*pGGD-mVENUS/ pD00587*	*pVL66*	*pVL53*	*pVL11*
BAM3:SMXL5-VENUS (pNT49)	*pNT48*	*pVL50*	*pVL84*	*pGGD-mVENUS/ pD00587*	*pVL66*	*pVL53*	*pVL11*
CVP2:SMXL5-VENUS (pNT16)	*pNT9*	*pVL50*	*pVL84*	*pGGD-mVENUS/ pD00587*	*pVL66*	*pVL53*	*pVL11*
APL:SMXL5-VENUS (pNT10)	*pVL35*	*pVL50*	*pVL84*	*pGGD-mVENUS/ pD00587*	*pVL25*	*pVL53*	*pVL11*
OPS:ER-VENUS (pNT53)	*pNT51*	*pVL63*	*pVL70*	*pVL71*	*pVL66*	*pVL53*	*pVL11*
BAM3:ER-VENUS (pNT50)	*pNT48*	*pVL63*	*pVL70*	*pVL71*	*pVL66*	*pVL53*	*pVL11*
CVP2:ER-VENUS (pNT69)	*pNT9*	*pVL63*	*pVL70*	*pVL71*	*pVL66*	*pVL53*	*pVL11*
APL:ER-VENUS (pNT68)	*pVL35*	*pVL63*	*pVL70*	*pVL71*	*pVL66*	*pVL53*	*pVL11*
SMXL4:BRX-VENUS (pNT72)	*pNT42*	*pVL50*	*pNT71*	*pGGD-mVENUS/ pD00587*	*pVL66*	*pVL53*	*pVL11*
SMXL5:OBE3-mTurquoise (pEW72)	*pVL28*	*pVL50*	*pVL85*	*pVL101*	*pVL20*	*pVL53*	*pVL11*
35S:5xc-Myc-OBE3 (pEW78)	*pDS34*	*pEW75*	*pVL85*	*pVL51*	*pVL66*	*pVL53*	*pVL11*
35S:SMXL5-mCherry (pVL122)	*pDS34*	*pVL50*	*pVL84*	*pVL119*	*pVL66*	*pVL53*	*pVL11*
35S:OBE3-mGFP (pVL127)	*pDS34*	*pVL50*	*pVL85*	*pVL69*	*pVL66*	*pVL53*	*pVL11*
35S:mCherry-NLS (pMG103)	*pGGA004/pDS34*	*pGGB003/pLV50*	*pGGC015*	*pGGD007*	*pGGE001/pVL66*	*pGGF007*	*pGGZ003/pVL11*
UBI10:mGFP-mCherry-NLS (pCW194)	*pGGA006*	*pCW192*	*pCW193*	*pGGD007*	*pGGE009*	*pGGF007*	*pGGZ003/pVL11*

Supplementary Table 3: Entry modules received for GreenGate cloning

List of received entry modules (for GreenGate Cloning)		
Name (see list)	**Construct**	**Reference**
pVL50	B-Dummy (pGGB003)	Lampropoulos et al. 2013
pGGD-mVENUS	pD00587	VENUS in Module D, Karin Schumacher
pVL66	Rbcs term (pGGE001)	Lampropoulos et al. 2013

bioRxiv preprint doi: https://doi.org/10.1101/2019.12.21.885863; this version posted December 23, 2019. The copyright holder for this preprint (which was not certified by peer review) is the author/funder, who has granted bioRxiv a license to display the preprint in perpetuity. It is made available under aCC-BY-NC 4.0 International license.

pVL53	SulfR (pGGF012)	Lampropoulos et al. 2013
pVL11	pGGZ003	Lampropoulos et al. 2013
pVL63	Signal Peptide (ER)	Lampropoulos et al. 2013
pVL70	YFP/VENUS (pGGC023)	Schuerholz, Lopez-Salmeron et al. 2018
pVL71	HDEL	Lampropoulos et al. 2013
pVL35	APL	Schuerholz, Lopez-Salmeron et al. 2018
pVL25	APL terminator	Schuerholz, Lopez-Salmeron et al. 2018
pVL28	pSMXL5	Schuerholz, Lopez-Salmeron et al. 2018
pVL101	pSW394	mTurquoise in Mod D, Sebastian Wolf
pVL20	SMXL5 terminator	Schuerholz, Lopez-Salmeron et al. 2018
pDS34	pGGA004	Lampropoulos et al. 2013
pVL51	D-Dummy (pGGD002)	Lampropoulos et al. 2013
pGGC015	mCherry	Lampropoulos et al. 2013
pGGD007	linker-NLS	Lampropoulos et al. 2013
pGGF007	KanR	Lampropoulos et al. 2013
pGGA006	pUBC10	Lampropoulos et al. 2013
pGGE009	UBC10 terminator	Lampropoulos et al. 2013
pVL119	mCherry (pGGD003)	Lampropoulos et al. 2013
pVL69	mGFP (pGGD001)	Lampropoulos et al. 2013

bioRxiv preprint doi: https://doi.org/10.1101/2019.12.21.885863; this version posted December 23, 2019. The copyright holder for this preprint (which was not certified by peer review) is the author/funder, who has granted bioRxiv a license to display the preprint in perpetuity. It is made available under aCC-BY-NC 4.0 International license.

Resource Table

RESOURCE	SOURCE	IDENTIFIER
Antibodies		
Anti-HA-Peroxidase High Affinity (3F10), rat monoclonal	Roche; Basel, Switzerland	Cat# 11867423001
c-Myc Antibody sc-40 HRP (9E10), mouse monoclonal	Santa Cruz Biotechnology, Santa Cruz, USA	Cat# sc-40
Bacterial and Virus Strains		
Agrobacterium tumefaciens C58C1: RifR with pSoup plasmid (TetR)	Ashby et al., 1988 Hellens et al., 2000	
Agrobacterium tumefaciens ASE: KanR, CamR with pSoup+ plasmid (TetR)	Merrit et al., 1999 Hellens et al., 2000	
Agrobacterium tumefaciens C58C1: RifR with *35S:P19*	Voinnet et al. 2013	
Chemicals, Peptides, and Recombinant Proteins		
DirectRed 23	Sigma-Aldrich; St. Louis, USA	Cat#212490
ClearSee	Kurihara et al. 2015	
Propidium iodide	Sigma-Aldrich; St. Louis, USA	Cat#81845
Nicotiana infiltration induction buffer (10 mM MES pH 5.5, 10 mM MgSO4, 150 µM Acetosyringone)	This paper	N/A
cOmplete™ Protease Inhibitor Cocktail	Sigma-Aldrich; St. Louis, USA	Cat#11697498001
Protein extraction buffer (50 nM Na_3PO_4, 150 mM NaCl, 10 % Glycerol, 5 mM EDTA, 10 µM β-mercaptoethanol, 0.1 % Triton X-100, 2 mM $NaVO_4$, 2 mM NaF, cOmplete tablet (1/2 tablet per 20ml), 20 µM MG132, 1 mM PMSF)	This paper	N/A
Wash buffer I (50 nM Na_3PO_4, 150 mM NaCl, 10 % Glycerol, 5 mM EDTA, 0.1 % triton X-100, 2 mM $NaVO_4$, 2 mM NaF, cOmplete tablet (1/2 tablet per 20ml), 20 µM MG132, 1 mM PMSF)	This paper	N/A
Wash buffer II (50 nM Na_3PO_4, 150 mM NaCl, 10 % Glycerol, 5 mM EDTA)	This paper	N/A
Sample Buffer, Laemmli 2x Concentrate	Sigma-Aldrich; St. Louis, USA	Cat#S3401
SuperSignal™ West Femto Maximum Sensitivity Substrate	Thermo-Scientific; Waltham, USA	Cat#34094
PageRuler™ Plus Prestained Protein Ladder, 10 to 250 kDa	Thermo-Scientific; Waltham, USA	Cat#26619
Bio-Rad Protein Assay Dye Reagent Concentrate	Bio-Rad Laboratories; Hercules, USA	Cat#5000006EDU

bioRxiv preprint doi: https://doi.org/10.1101/2019.12.21.885863; this version posted December 23, 2019. The copyright holder for this preprint (which was not certified by peer review) is the author/funder, who has granted bioRxiv a license to display the preprint in perpetuity. It is made available under aCC-BY-NC 4.0 International license.

Experimental Models: Organisms/Strains		
Arabidopsis: wild type Col-0	Gudrun Böhmdorfer	
Arabidopsis: *smxl5-1 (SALK_018522)*	Wallner et al. 2017	N/A
Arabidopsis: *smxl4-1 (SALK_037136)*	Wallner et al. 2017	N/A
Arabidopsis: *smxl3-1 (SALK_024706)*	Wallner et al. 2017	N/A
Arabidopsis: *obe1-1 (SALK_075710)*	Saiga et al. 2008	N/A
Arabidopsis: *obe2-1 (KG16805)*	Saiga et al. 2008	N/A
Arabidopsis: *obe3-2/tta1-2 (SALK_042597)*	Saiga et al. 2012	N/A
Arabidopsis: *obe4-1/tta2-1 (SALK_082338)*	Saiga et al. 2012	N/A
Arabidopsis: *smxl4-1 smxl5-1 (SALK_037136, SALK_018522)*	Wallner et al. 2017	N/A
Arabidopsis: *smxl4-1 obe1-1 (SALK_037136, SALK_075710)*	This paper	N/A
Arabidopsis: *smxl5-1 obe1-1 (SALK_018522, SALK_075710)*	This paper	N/A
Arabidopsis: *smxl4-1 obe2-1 (SALK_037136, KG16805)*	This paper	N/A
Arabidopsis: *smxl5-1 obe2-1 (SALK_018522, KG16805)*	This paper	N/A
Arabidopsis: *smxl4-1 obe3-2 (SALK_037136, SALK_042597)*	This paper	N/A
Arabidopsis: *smxl5-1 obe3-2 (SALK_018522, SALK_042597)*	This paper	N/A
Arabidopsis: *smxl3-1 obe3-2 (SALK_024706, SALK_042597)*	This paper	N/A
Arabidopsis: *smxl4-1 obe4-1 (SALK_037136, SALK_082338)*	This paper	N/A
Arabidopsis: *smxl5-1 obe4-1(SALK_018522, SALK_082338)*	This paper	N/A
Arabidopsis: brx-2 (pSKI15)	Rodrigues et al. 2009	N/A
Arabidopsis: ops-2 (SALK_139316)	Truernit et al. 2012	N/A
Arabidopsis: brx-2 smxl5-1 (pSKI15, SALK_018522)	This paper	N/A
Arabidopsis: ops-2 smxl5-1 (SALK_139316, SALK_018522)	This paper	N/A
Arabidopsis: *SMXL4:SMXL4-YFP* in wild type	Wallner et al. 2017	N/A
Arabidopsis: *OBE3:OBE3-GFP/TTA1:TTA1-GFP* in wild type	Saiga et al. 2012	N/A
Arabidopsis: *OBE4:OBE4-GFP/TTA2:TTA2-GFP* in wild type	Saiga et al. 2012	N/A
Arabidopsis: SMXL5:OBE3-turquoise in *smxl5-1 obe3-2 (SALK_018522, SALK_042597)*	This paper	N/A
Arabidopsis: SMXL5:obe3-miRNA3 in *smxl5-1 (SALK_018522)*	This paper	N/A
Arabidopsis: SMXL5:obe3-miRNA4 in *smxl5-1 (SALK_018522)*	This paper	N/A
Arabidopsis: OPS:SMXL5-VENUS (pNT52) in *smxl4-1 smxl5-1 (SALK_037136, SALK_018522)*	This paper	N/A
OPS:ER-VENUS (pNT53) in wild type	This paper	N/A

bioRxiv preprint doi: https://doi.org/10.1101/2019.12.21.885863; this version posted December 23, 2019. The copyright holder for this preprint (which was not certified by peer review) is the author/funder, who has granted bioRxiv a license to display the preprint in perpetuity. It is made available under aCC-BY-NC 4.0 International license.

BAM3:SMXL5-VENUS (pNT49) in *smxl4-1 smxl5-1 (SALK_037136, SALK_018522)*	This paper	N/A
BAM3:ER-VENUS (pNT50) in wild type	This paper	N/A
CVP2:SMXL5-VENUS (pNT16) in *smxl4-1 smxl5-1 (SALK_037136, SALK_018522)*	This paper	N/A
CVP2:ER-VENUS (pNT69) in wild type	This paper	N/A
APL:SMXL5-VENUS (pNT10) in *smxl4-1 smxl5-1 (SALK_037136, SALK_018522)*	This paper	N/A
APL:ER-VENUS (pNT68) in wild type	This paper	N/A
SMXL4:BRX-VENUS (pNT72) in *smxl4-1 smxl5-1 (SALK_037136, SALK_018522)*	This paper	N/A
OPS:OPS-GFP in wild type	Rodriguez-Villalon et al. 2014	N/A
OPS:OPS-mGFP6 in *smxl4-1 smxl5-1 (SALK_037136, SALK_018522)*	This paper	N/A
BRX:BRX-CITRINE in wild type	Rodriguez-Villalon et al. 2014	N/A
BRX:BRX- CITRINE in *smxl4-1 smxl5-1 (SALK_037136, SALK_018522)*	This paper	N/A
BAM3:BAM3- CITRINE in wild type	Rodriguez-Villalon et al. 2014	N/A
BAM3:BAM3- CITRINE in *smxl4-1 smxl5-1 (SALK_037136, SALK_018522)*	This paper	N/A
CVP2:NLS-VENUS in wild type	Rodriguez-Villalon et al. 2014	N/A
CVP2:NLS-VENUS in *smxl4-1 smxl5-1 (SALK_037136, SALK_018522)*	This paper	N/A
Nicotiana benthamiana	Karin Schumacher	N/A
Saccharomyces cerevisiae: AH109 (MATa, trp1-901, leu2-3, 112, ura3-52, his3-200, gal4Δ, gal80Δ, LYS2 : : GAL1UAS-GAL1TATA-HIS3, GAL2UAS-GAL2TATA-ADE2, URA3 : : MEL1UAS-MEL1 TATA-lacZ)	Armin Djamei Matchmaker™ Two-Hybrid System 3 (Clontech, Palo Alto)	https://www.takarabio.com/assets/documents/User%20Manual/PT3247-1.pdf
Recombinant DNA		
35S:SMXL5-3xHA	This paper	pEW33
35S:6xc-Myc-OBE3	This paper	*pEW78*
35S:*OBE3-mGFP*	This paper	*pVL127*
35S:SMXL5-mCherry	This paper	*pVL122*
UBI10:mGFP-mCherry-NLS	This paper	*pCW194*
35S:mCherry-NLS	This paper	*pMG103*
SMXL5:OBE3-miRNA3	This paper	*pEW65*
SMXL5:OBE3-miRNA4	This paper	*pEW66*
SMXL4:SMXL4-YFP (+ 3' *SMXL4* terminator)	Wallner et al. 2017	*pEW23*
SMXL5:OBE3-turquoise	This paper	*pEW72*
OPS:SMXL5-VENUS	This paper	*pNT52*
OPS:ER-VENUS	This paper	*pNT53*
BAM3:SMXL5-VENUS	This paper	*pNT49*
BAM3:ER-VENUS	This paper	*pNT50*
CVP2:SMXL5-VENUS	This paper	*pNT16*

bioRxiv preprint doi: https://doi.org/10.1101/2019.12.21.885863; this version posted December 23, 2019. The copyright holder for this preprint (which was not certified by peer review) is the author/funder, who has granted bioRxiv a license to display the preprint in perpetuity. It is made available under aCC-BY-NC 4.0 International license.

CVP2:ER-VENUS	This paper	*pNT69*
APL:SMXL5-VENUS	This paper	*pNT10*
APL:ER-VENUS	This paper	*pNT68*
SMXL4:BRX-VENUS	This paper	*pNT72*
BRX:BRX-CITRINE	Rodriguez-Villalon et al. 2014	*N/A*
Software		
WMD3 – Web MicroRNA Designer Version 3	Max Planck Institute for Developmental Biology, Tübingen.	http://www.weigelworld.org
CLC Main Workbench 7.6.1	CLC Bio Qiagen, Aarhus, Denmark	
ImageJ 1.51h	National Institute of Health, Bethesda, USA	
Microsoft Office 2016	Microsoft, Redmond, USA	
Adobe Creative Suite CS6	Adobe, San Jose, USA	
SPSS V. 25	IBM, Armonk, USA	
GraphPad Prism version 6.01	GraphPad Software, La Jolla, USA	
Other		
Anti-HA MicroBeads	Miltenyi Biotec, Bergisch Gladbach, Germany	Cat#130-094-255
µ Columns	Miltenyi Biotec, Bergisch Gladbach, Germany	Cat#130-042-701
Advanced Fluorescence and ECL Imager	Intas Science Imaging Instruments, Göttingen, Germany	N/A
Confocal microscope TCS SP5	Leica Microsystems; Mannheim, Germany	N/A
Confocal microscope TCS SP8	Leica Microsystems; Mannheim, Germany	N/A